Preliminary Design of the Cratus Air Racer

2011-2012 AIAA Individual Aircraft Design Competition

Samantha Schueler

Instructor: Dr. Ron Barrett

THE UNIVERSITY OF KANSAS

Department of Aerospace Engineering

10 June 2012

Preliminary Design of the Cratus Air Racer

Designer: Samantha Schueler

AIAA Member ID: 432318

Faculty Advisor: Dr. Ron Barrett

Acknowledgements

The author would like to thank Mr. Josh Brungart, Mr. Perry Rea, and Dr. Ron Barrett for their insight into Reno racing and aircraft design. Also, a special thanks to Mr. Christopher Herling and Mr. Alan Nguyen for their support throughout the design of the Cratus.

Table of Contents

Page #

Table of Contents (continued)

List of Figures

List of Figures (continued)

List of Tables

List of Symbols

Symbol	Description	Units
A, AR	Aspect Ratio	~
A	Regression Line Constant	~
b	Span	ft
B	Regression Line Constant	~
c	Chord Length	ft
c_p	Specific Fuel Consumption	lbf/hp/hr
C_D	Coefficient of Drag	~
C_{D_0}	Parasite Drag Coefficient	~
C_L	Coefficient of Lift	~
C_{n_β}	Yawing Moment Coefficient Due to Sideslip	1/deg
d	Diameter	ft
D	Drag	lbf
e	Oswald's Efficiency Factor	~
E	Endurance	hr
F	Sensitivity Constant	~
F	Force	lbf
h	Height	ft
i	Incidence Angle	deg
J	Advance Ratio	~
l	Length	ft

List of Symbols (continued)

L	Lift	lbf
M_{ff}	Mission Fuel Fraction	~
n	Load Factor	~
P	Power	hp
R	Range	nm
S	Area	ft^2
t	Thickness	ft
t/c	Thickness to Chord Ratio	~
V	Velocity	ft/s
w	Width	ft
W	Weight	lbf
W/P	Power Loading	lbf/hp
W/S	Wing Loading	lbf/ft^2

Greek Symbols

Γ	Dihedral Angle	deg
ε	Geometric Twist	deg
Λ	Sweep Angle	deg
λ	Taper Ratio	~
η	Span Wise Station	~
η	Efficiency	~
θ	Angle	deg

Subscripts

apu..... Auxiliary Power Unit

bl ..... Blade

c/4 ..... Quarter Chord

crew..... Crew

cruise.....Cruise

DYN..... Dynamic

e.....Elevator

e..... Exhaust

E ..... Empty

els.....Electrical System

emp ..... Empennage

f ..... Fuel

f .....Fuselage

fc .....Fuselage Cone

fur..... Furnishings

fwd .....Forward

h ..... Horizontal

hps.....Hydraulic Power System

i .....Inboard

iae..... Instrumentation, Avionics, and Electronics

int ..... Interference

Subscripts (continued)

L ..... Landing

m ..... Main

max ..... Maximum

n ..... Nose

o ..... Outboard

p ..... Propeller

pc..... Propulsion Control

r ..... Root

r ..... Rudder

res..... Reserves

s ..... Strut

t ..... Tip

t ..... Tire

tfo ..... Trapped Fuel and Oil

TO ..... Takeoff

ult ..... Ultimate

v ..... Vertical

w ..... Wing

wet..... Wetted

wi ..... Water Injection

Acronyms

AAA..... Advanced Aircraft Analysis

AC.....Aerodynamic Center

AIAA ..... American Institute of Aeronautics and Astronautics

CG.....Center of Gravity

NACA .....National Advisory Committee for Aeronautics

RFP .....Request for Proposal

SM.....Static Margin

1 Introduction

1.1 Reno Racing

The Reno Races are an annual competition held at the Reno Stead Airport, comprised of six classes of aircraft: Unlimited, Jet, Sport, T-6, Biplane, and Formula One (Ref. 1). The design of the Cratus is for the Unlimited Class race which is currently dominated by modified World War II aircraft. These modifications include but are not limited to: wingspan reduction, increase in engine power output, increased cooling capability, and drag reduction through skin surface smoothing.

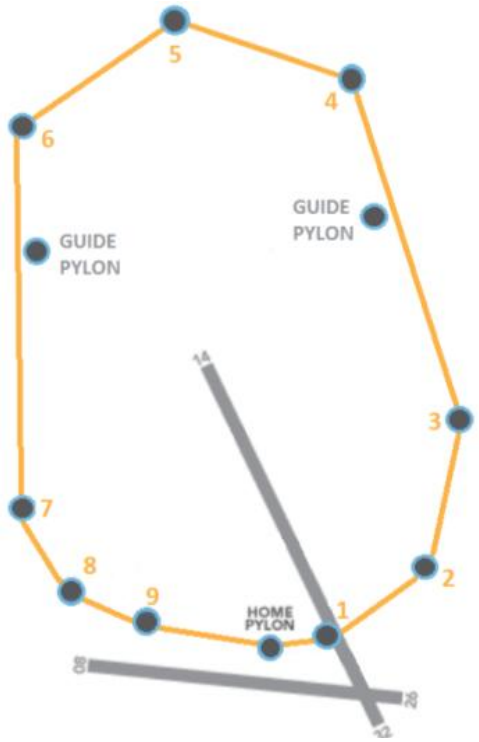

Figure 1.1: Reno Race Course

According to the RFP, the aircraft must have a minimum empty weight of no less than 4,500 lbf, be able to pull a 6 g turn, be competitive with the best current racers, and be piston-driven (Ref. 2).

The race course on which the race takes place is roughly 8.4 miles. Figure 1.1 and 1.2 show the race course and the mission profile for the race mission, respectively. One requirement of every Unlimited Class racer is the ability to complete a 500 nmi ferry mission.

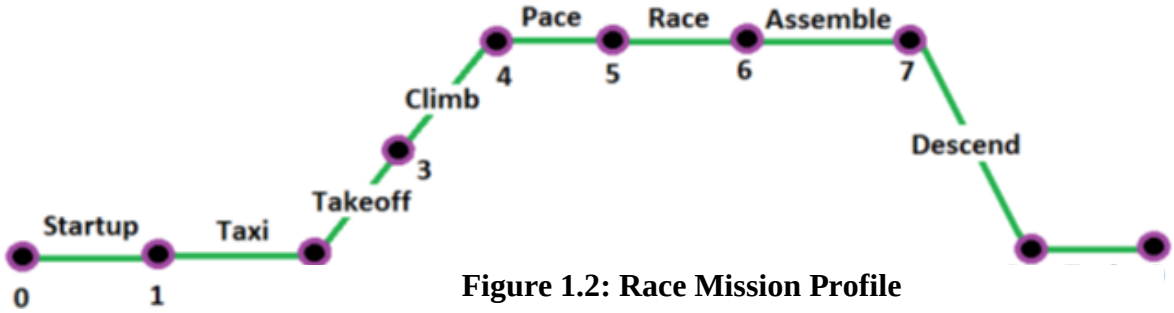

Figure 1.2: Race Mission Profile

1.2 Phasing of Tasks

The design process for the Cratus is shown in Figure 1.3. It was divided into five major phases as shown below:

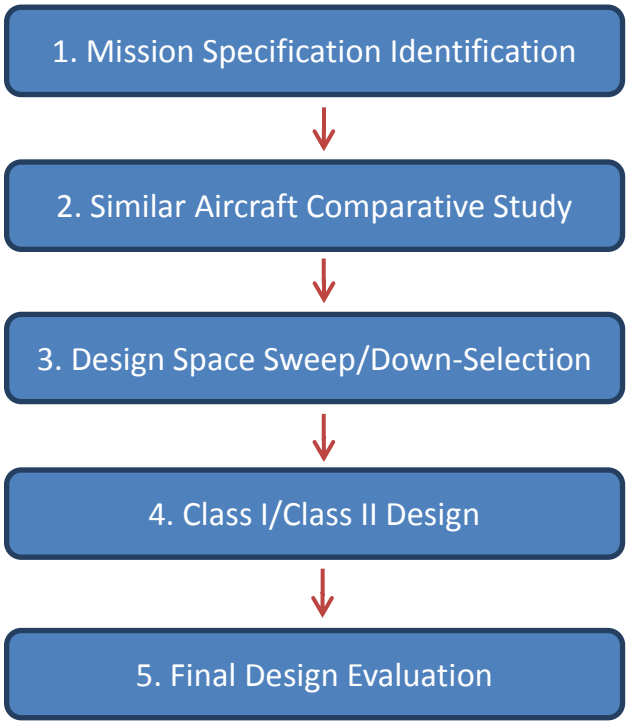

Figure 1.3: Phasing of Tasks

1. **Mission Specification and Identification**

   Based on the RFP (Ref. 2) and current Unlimited Class Reno Racing rules, the mission specification and mission profile was determined. These were stated in Section 1.1.

2. **Similar Aircraft Comparative Study**

   Aircraft currently used in the Unlimited Class race were compared based on their design specifications and flight performance. This allowed for an accurate basis on which to design the Cratus, considering the requirement that it must be able to outperform current racers.

3. **Design Space Sweep/Down-Selection**

   Viable aircraft configurations were considered and analyzed in a comparative study allowing for the optimal configuration to be identified. This also provided a down-selection of the design space to focus the design analysis.

4. **Class I/Class II Design**

   Class I design secured the preliminary design of the Cratus. This was followed by Class II design which produced a more finite analysis of the aircraft.

5. **Final Design Evaluation**

   During the final design evaluation, an assessment was made of whether the design meets the requirements of the mission specification and any additional stipulations placed on the aircraft, such as safety.

1.3 Design Philosophy

The primary goal of the Cratus is safety. Due to recent events, the emphasis that safety should have on Reno racer designs has been made apparent. Following research into what pilots' fear most during flight, the focus for safety became fire prevention and suppression and pilot visibility and spatial awareness (Ref. 3). By focusing on these areas of safety, extra weight was not added for unnecessary systems.

Eliminating unnecessary systems assisted in not exceeding the minimum empty weight of 4,500 lbf. It also helped to keep the complexity of the aircraft as low as possible, increasing the reliability of the aircraft as well as reducing the opportunity for pilot error due to over complication. By meeting, but not exceeding, the minimum empty weight requirement, the maneuverability and speed of the aircraft was increased.

The philosophy adopted by the Cratus to surpass all other racers was more thrust and less drag. This is common of many current racers leading to drastic aircraft modifications (engine modifications for more power, skin smoothing, and wingspan reduction). The difference between current racers and the Cratus is technological improvements. Current racers are unable to optimize their aircrafts using current technology and materials, such as composites, without creating a new aircraft; therefore they are limited by the basic structure and composition of their aircraft. Designing the Cratus first and foremost as a Reno racer gives it a distinct advantage because each design decision was made for the sole purpose of winning races.

1.4 Design Methods

Throughout the design process, both the program Advanced Aircraft Analysis and Microsoft Excel were used. A model was created using AAA and then checked using Excel to verify the values attained. The Excel code created by the author followed the procedure detailed in Dr. Jan Roskam's Aircraft Design Series (Ref. 4), therefore all values found using AAA and Excel should, theoretically, be comparable. This was found to be true throughout the design process with negligible differences between the two.

2 Technical Approach to Meet Mission Requirements

The primary validation behind decisions was safety. The history of the Reno Races has proven it to be a dangerous sport, therefore it was deemed reasonable to make safety a primary focus. Following safety, meeting the design requirements was the second-most important factor in the design process. Without meeting the requirements laid out in the RFP (Ref. 2), the design would be forfeit.

2.1 Safety Aspects

Reno racing aircraft have very different safety concerns with respect to typical, commercially available aircraft. This is due mainly to the conditions to which these aircraft are exposed. The low-flight altitude and high speeds are a deadly combination which result in reduced reaction times in high risk situations. To prepare for this, a fully-enclosed cockpit with ejection system was considered to provide debris protection and pilot evacuation in the event that ground impact is unavoidable. Following a discussion with a Reno Race pilot, this was considered an unreasonable safety precaution because the risk of inverted flight and direct ejection into the ground is high and it is not a realistic expectation for the pilot to be able to eject successfully in the time-frame of a race following a malfunction (Ref. 3). The chief safety concerns of pilots

Figure 2.1: Low-Flying Reno Racer[5]

during races are a cockpit fire and collision with other racers. With this insight, the Cratus focuses on minimizing these risks in order to decrease weight and complexity.

2.1.1 Fire Safety

A personal fire extinguisher will be attached to the base of the pilot's chair for easy accessibility and convenience. In the event of a cockpit fire, this will be used for the pilot's personal protection. Two ventilation systems were designed for pilot safety after the use of the fire extinguisher within the cockpit. The first is the less severe of the two, with simple ventilation holes which can be opened with a simple lever next to the pilot. The second system releases the entire canopy. The cockpit is designed with a side hinge canopy; this allows for, in the case of an emergency, the hinge pin to be removed and the canopy to be pushed off by the pilot.

By using the fire extinguisher and then immediately opening a ventilation system, the fire suppressant will evacuate the cockpit due to the differential pressure between the inside of the cockpit and the outside air pressure. Having the two ventilation systems gives the pilot the option to keep the aircraft in a flying condition if the fire is minor. This allows time to land the aircraft safely, if the pilot deems it possible. The removable canopy ensures expedient pilot evacuation if necessary.

2.1.2 Racer Collision Avoidance

The fast-paced Reno Races are ripe with opportunities for collision, not only with the ground, but other racers. The spatial awareness of each pilot is the only separation between each aircraft, showing the importance of clear line of sight for the pilot of the Cratus. A head-up display unit was considered, but following a discussion with a current Reno racer the concept was dismissed due to pilot preference for seeing the actual surroundings of the aircraft instead of a screen (Ref. 3). The vital areas for clear vision are above and behind the pilot's left shoulder and the lower

right side of the cockpit (Ref. 3). These areas are extremely important during maneuvers around pylons and other aircraft.

To meet these requirements, a high-strength polycarbonate material will be used for the cockpit canopy. Polycarbonates have been proven an effective material for cockpit applications through its use on many aircraft, including the F-22, F-16, Boeing 787, and many others.

Figure 2.2: Reno Racers Near Pylon[5]

2.1.3 Propeller and Engine Location

The propeller is located forward and aft of the cockpit for several safety reasons. The most important is in case a propeller blade is thrown. In 1956, a blade was thrown on a Vickers Viscount 700 (Ref. 6). It cut into the cabin killing one and injuring five. If a blade is thrown on the Cratus, worst case, it will bisect the fuselage, completely avoiding the cockpit and pilot. Locating the two main engines aft of the cockpit assists in cockpit noise control. The National Institute for Occupational Safety and Health released a study relating background noise to general stress levels and aggravation of stress-related conditions (Ref. 7). Reno Race pilots are already performing in a high stress environment, therefore increased cockpit noise from the engines and propellers would only exacerbate the effect.

The use of three engines introduces the safety hazard of one engine inoperable flight. The yawing moment the aircraft would experience would likely be irrecoverable considering the low altitude and high speed flight during race conditions. To improve the chances of recovery, the Cratus will contain an electrical feathering system. If one wing engine losses thrust output, the

wing engine propellers will automatically feather to reduce the drag experienced by the inoperable engine. The pilot will then be able to land the aircraft safely with the remaining forward engine. If the forward engine becomes inoperable during flight, the aircraft can safely land using the remaining two wing engines.

2.2 Technical Aspects

The main goals of a racer are speed and maneuverability. These goals were addressed through drag reduction techniques, high wing loading, and high power loading. The general theory tracked throughout the design of the Cratus was minimizing wetted area and frontal area.

The inverse gull wing design has several purposes. The first is to reduce landing gear length which reduces the landing gear weight and retraction volume. This allows for the internal volume of the aircraft to be used for fuel and water storage necessary for flight. The wing design also gives the aircraft more favorable stall properties. The sweep of the wing induces root stall prior to tip stall allowing prolonged aileron effectiveness. The mid-wing engine cowlings act as wing fences preventing the entire wing from stalling simultaneously.

The airfoil chosen for the wing is supercritical to minimize drag. The supercritical shape delays the onset of wave drag which will have a significant impact on the aircraft due to the transonic race speeds.

The empty weight of the aircraft is minimized to also minimize the loaded weight of the aircraft, thereby increasing the maneuverability. Deciding on a high wing loading and power loading reduces the wetted area of the aircraft and the power required to complete the desired mission.

2.3 Similar Aircraft

The mission requirement states that the aircraft design must be capable of outperforming current racers. To ensure this constraint is met, a comparison of existing racers was completed. This is shown in Table 2.1.

Table 2.1: Similar Aircraft[8]

Aircraft	W_E (lbf)	W_{TO} (lbf)	P (hp)	V_{max} (mph)
P-51	7,635	12,100	1,490	437
F4U	8,982	14,000	2,000	417
Sea Fury	9,240	12,500	2,480	460
F7F	16,270	25,720	4,200	460
Spitfire	5,090	6,622	1,470	378
P-38	12,800	21,600	3,450	443

3 Class I and II Sizing Methods and Sensitivities

Preliminary sizing of the Cratus provides the first comparison of existing aircraft to theoretically viable aircraft sizes. The design space is narrowed based on the flight requirements defined by the Reno Racing rules (Ref. 1). This is shown in the following sections including: mission weight estimates, weight sizing, and performance constraints.

3.1 Mission Weight Estimates

The following weights were assumed to attain a preliminary estimate for the aircraft take-off weight:

- W_E=4,500 lbf
- W_{tfo}=0.5% W_{TO}
- W_{crew}=150 lbf
- W_{PL}=0 lbf

$$W_{TO} = W_E + W_{tfo} + W_F + W_{crew} + W_{PL}$$

(Eq. 2.1, Ref. 9) **Equation 3.1**

The calculation of the mission fuel weight was completed using the mission fuel-fraction method. Since the Cratus has two missions, race and ferry, the fuel determining mission was determined by finding the mission which required the most fuel. Calculation of the cruise, pace, race, and assembly mission segment fuel-fractions were completed using the Breguet Range and Endurance equations. These can be seen below:

$$R\ (nmi) = 375\left(\frac{nmi - lbf}{hp - hr}\right)\left(\frac{\eta_p}{c_p\left(\frac{lbf}{hp - hr}\right)}\right)\left(\frac{L}{D}\right) ln\left(\frac{1}{M_{ff_i}}\right)$$

(Eq. 2.9, Ref. 9) **Equation 3.2**

$$E\ (hr) = 375\left(\frac{nmi - lbf}{hp - hr}\right)\left(\frac{1}{V\ (kts)}\right)\left(\frac{\eta_p}{c_p\left(\frac{lbf}{hp - hr}\right)}\right)\left(\frac{L}{D}\right)ln\left(\frac{1}{M_{ff_i}}\right)$$

(Eq. 2.11, Ref. 9) **Equation 3.3**

The assumptions made for each of the four previously mentioned segments are shown in Table 3.1.

Table 3.1: Mission Fuel Fraction Assumptions

Mission Segment	R (nm)	E (hr)	V (kts)	η_p (~)	c_p (lbf/hp-hr)	L/D (~)
Cruise	500	~	~	0.7	0.6	5
Pace	~	0.167	300	0.7	0.6	5
Race	~	0.128	500	0.7	1.55	2
Assembly	~	0.133	200	0.7	0.6	5

The final mission fuel-fractions for each segment in both the race and ferry mission are shown in Table 3.2.

Table 3.2: Mission Fuel Fractions

Mission Segment		Segment Number	M_{ff}	
Ferry	**Race**		**Ferry**	**Race**
Warm-up	Warm-up	1	0.99	0.99
Taxi	Taxi	2	0.99	0.99
Takeoff	Takeoff	3	0.99	0.99
Climb	Climb	4	0.96	0.999
Cruise	Pace	5	0.769	0.974
Descent	Race	6	0.99	0.807
Land/Taxi	Assembly	7	0.995	0.983
~	Descent	8	~	0.999
~	Land/Taxi	9	~	0.995
M_{ff}			**0.706**	**0.745**

From the mission fuel fractions above, it is apparent that the ferry mission is the fuel critical mission. Therefore, it will determine the minimum amount of fuel which must be carried onboard the aircraft. The ferry mission required fuel weight is calculated using the following equation:

$$W_F = \left(1 - M_{ff}\right)W_{TO} = 0.294W_{TO}$$

(Eq. 2.14, Ref. 9) **Equation 3.4**

From Equation 3.4:

$$W_{TO} = 6{,}381\ lbf$$

$$W_F = 1{,}881\ lbf$$

3.2 Weight Regression

A weight regression line was created based on the empty and take-off weights of similar aircraft. This regression line is shown in Figure 3.1 along with the preliminary design point. The design point was defined by the preliminary weight calculations shown previously, in Section 3.1.

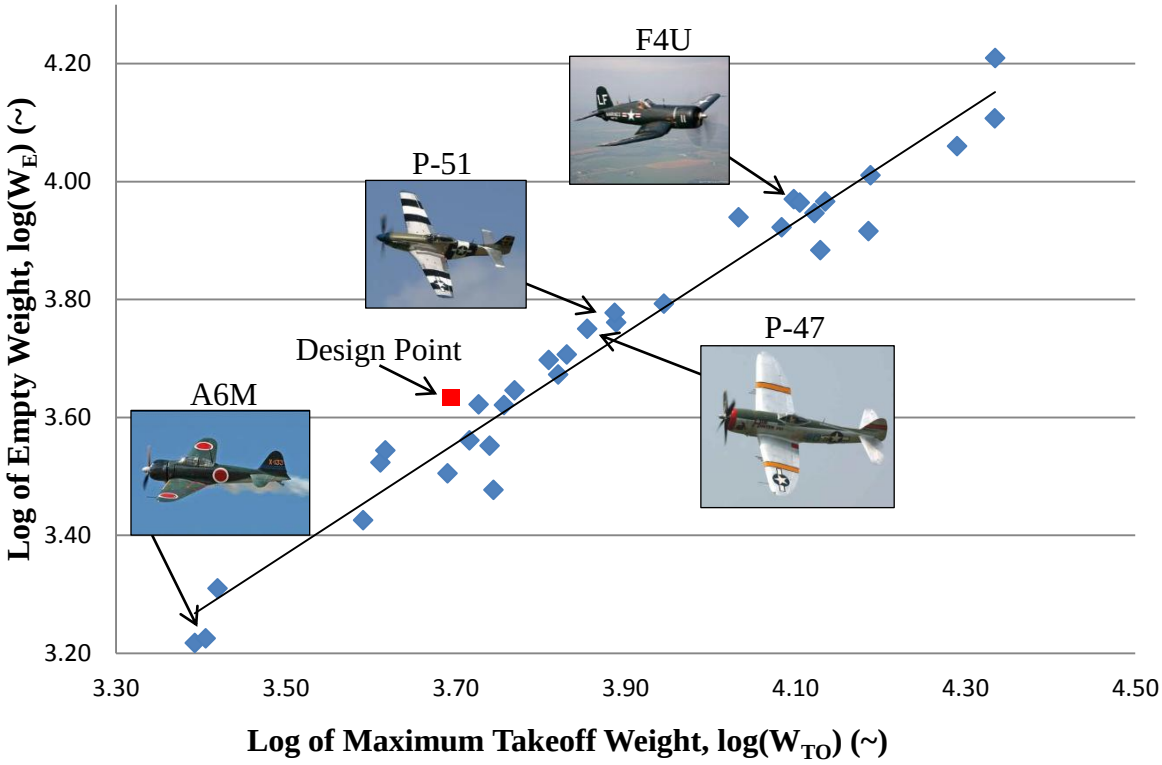

Figure 3.1: Weight Trend for Similar Aircraft

Figure 3.1 shows that the design point for the Cratus is above the trend line of similar aircraft. This is ideal because it means the take-off weight is lower than similar aircraft. This is because no additional weight, other than the pilot and fuel, was added.

3.3 Take-off Weight Sensitivities

The effect on each design assumption, with respect to take-off weight of the aircraft, was calculated. This was done to figure which design assumptions had the largest impact on the take-off weight of the aircraft. This information assists in effectively minimizing aircraft take-off weight. The following equations were used:

$$log_{10}W_{TO} = A + Blog_{10}(CW_{TO} - D)$$

(Eq. 2.24, Ref. 9) **Equation 3.5**

$$C = \left[1 - (1 + M_{res})\left(1 - M_{ff}\right) - M_{tfo}\right]$$

(Eq. 2.22, Ref. 9) **Equation 3.6**

$$D = W_{PL} + W_{crew} + W_{P_{exp}}$$

(Eq. 2.23, Ref. 9) **Equation 3.7**

$$F = -BW_{TO}^2(CW_{TO}[1 - B] - D)^{-1}(1 + M_{res})M_{ff}$$

(Eq. 2.44, Ref. 9) **Equation 3.8**

Table 3.3: Sensitivity Equations

Sensitivity	Equation	Value	Source
W_{TO} to W_E	$\frac{\partial W_{TO}}{\partial W_E} = BW_{TO}\left[10^{\frac{logW_{TO}-A}{B}}\right]^{-1}$	+1.1	(Eq. 2.27, Ref. 9) **Equation 3.9**
W_{TO} to c_p	$\frac{\partial W_{TO}}{\partial c_p} = FR\left[375\eta_p\frac{L}{D}\right]^{-1}$	+170 hp-hr	(Eq. 2.49, Ref. 9) **Equation 3.10**
W_{TO} to L/D	$\frac{\partial W_{TO}}{\partial \frac{L}{D}} = -FRc_p\left[375\eta_p\left(\frac{L}{D}\right)^2\right]^{-1}$	-20 lbf	(Eq. 2.51, Ref. 9) **Equation 3.11**
W_{TO} to R	$\frac{\partial W_{TO}}{\partial R} = Fc_p\left[375\eta_p\frac{L}{D}\right]^{-1}$	+10 lbf/hr	(Eq. 2.45, Ref. 9) **Equation 3.12**
W_{TO} to η_p	$\frac{\partial W_{TO}}{\partial \eta_p} = -FRc_p\left[375\eta_p^2\frac{L}{D}\right]^{-1}$	-110 lbf	(Eq. 2.50, Ref. 9) **Equation 3.13**

Table 3.4 shows the percent change in the take-off weight of the aircraft when each parameter is changed. These calculations were made assuming a linear relationship when the perturbation is small relation to the parameter.

Table 3.4: Design Parameter Impact on Take-off Weight

Parameter	Sensitivity	Parameter Change	Change in W_{TO} (lbf)	% Change in W_{TO}
W_E	+1.1	+5 lbf	5.5	0.08
c_p	+170 hp-hr	$+ 0.1 \frac{lbf}{hp - hr}$	17	0.26
L/D	-20 lbf	+1	-20	-0.3
R	+10 lbf/hr	+0.1 hr	1	0.015
η_p	-110 lbf	+10%	-11	-0.2

It can be concluded that take-off weight is most sensitive to changes in L/D, specific fuel consumption, and propeller efficiency.

3.4 Performance Constraints

The power loading and wing loading for the Cratus were found using a performance graph generated following the procedure outlined in Reference 9. The constraints which are defined in the RFP (Ref. 2) include: stall speed, take-off distance, landing distance, maneuvering capability, and flight speed. From the performance graph the limiting constraints which determined the Cratus' performance include: stall speed, maneuver capability, and $C_{L_{max}}$. The performance graph and design point are shown in Figure 3.2.

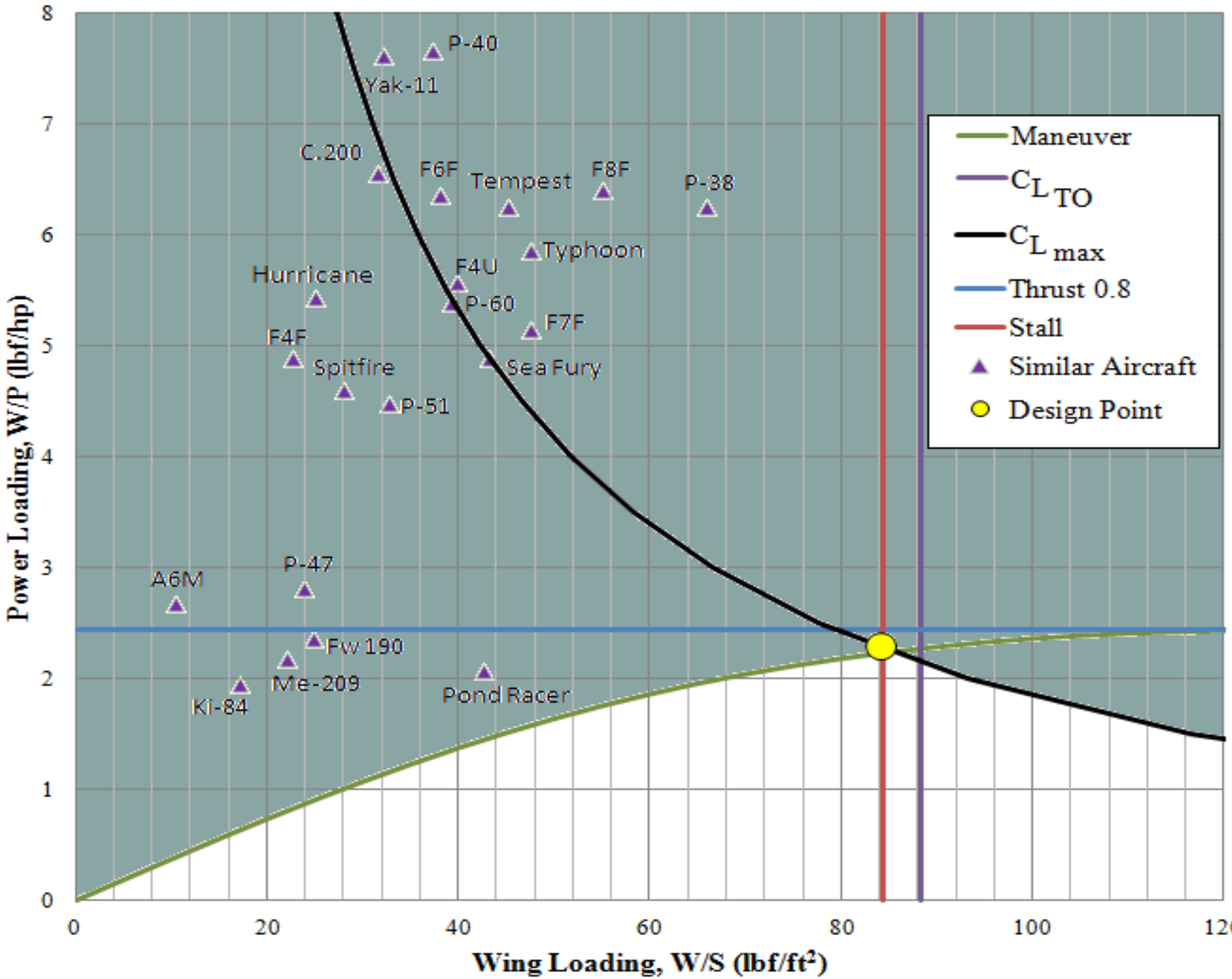

Figure 3.2: Performance Graph

The chosen design point has a power loading of 2.3 lbf/hp and a wing loading of 84.1 lbf/ft^2. Figure 3.2 shows that the power loading was chosen at the maximum value attainable with the given constraints. This is an important point since it defines the required horsepower of the aircraft based on weight. The figure also shows that the chosen wing loading is significantly higher than many similar aircraft. This was done to decrease the required wing area of the aircraft to increase its maneuverability. Due to advancements in aircraft materials, this wing loading is plausible.

4 Configuration and Three-View

4.1 Fuselage Configuration

The fuselage of the Cratus is a conventional design aimed to minimize wetted area. To do this, the fuselage was designed to wrap closely around the pilot, then taper towards the empennage. This approach minimizes the frontal area of the cockpit, as well as wetted area. The dimensions of the design are listed in Table 4.1.

Table 4.1: Fuselage Characteristics

Characteristic	Value
l_f	23.7 ft
d_f	5.1 ft
l_{fc}	10.3 ft
l_f/d_f	4.65
l_{fc}/d_f	2.01
θ_{fc}	38 deg

The fuselage was also designed with safety in mind. The fuel located within the fuselage was minimized to reduce the risk of fuel coming into contact with the pilot in the event of a crash. The water used for engine cooling is located below the cockpit and fuel tank. This was done as a safety feature in case an emergency landing is made without the deployment of the landing gear. If the underside of the fuselage is comprised the water will provide an additional layer of protection for the pilot if a fire is ignited. This is shown below in Figure 4.1.

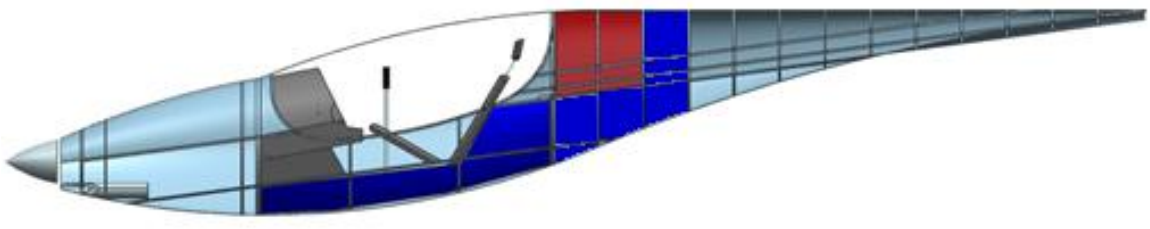

Figure 4.1: Fuselage Layout

4.2 Wing Configuration

A low, inverse-gull wing design was chosen for the Cratus for several reasons. The low wing assists in pilot visibility by removing the wing structure from the pilot's line of sight in the upper, left-hand, back corner. This visibility is needed to see other aircraft flying in close proximity to the Cratus.

The reasoning behind the polyhedral was landing gear length and weight and drag. The polyhedral lowers the waterline of the landing gear connection point. This decrease in length in turn lowers the weight of the landing gear and also minimizes the area required within the aircraft structure for gear retraction. The anhedral of the root section reduces the drag of the aircraft through a reduction of interference drag.

Table 4.2: Wing Characteristics

Characteristic	Value
S	56.8 ft^2
AR	15.3
$\Lambda_{c/4}$	-14.7 deg
t/c	10.7%
λ	0.3
i_w	0 deg
ε_t	0 deg
Γ_i	-13 deg
Γ_o	27 deg
Aileron Span Ratio	25%
Airfoil	SC(2)-0714

The sweep of the wing was designed for propeller clearance and stall behavior. The wing engines are in a pusher configuration, locating the propeller along the trailing edge of the wing. The aft swept root section and forward swept tip section allows for sufficient propeller clearance. The forward swept tip section also provides favorable stall characteristics during high angle of attack flight. The root section will theoretically stall prior to the tip keeping control of the aircraft through the use of the ailerons. The engine cowling locations on the wings also assist in the favorable stall characteristics by acting as stall fences to prevent premature tip stall. The dimensional characteristics of the wing are listed in Table 4.2.

4.3 Engine Configuration

The tri-engine configuration was chosen for increased power. Locating the two wing engines in a pusher configuration increases the performance of the wing section forward of the propeller. Although the nose engine is inherently destabilizing, locating the two engines on the wings inherently stabilizes the aircraft due to the location with regards to the aircraft center of gravity.

4.4 Empennage Configuration

The Cratus was designed with a v-tail to maintain the goals of the aircraft, performance and safety. The use of a v-tail allows for a reduction in weight of the empennage structure. While a conventional tail requires the structural elements to join three surfaces to the fuselage, a v-tail only requires the joining of two empennage surfaces. A v-tail also results in decreased drag. This comes from both a decrease in wetted area as well as a reduction in interference drag.

Table 4.3: Empennage Characteristics

S	5.58 ft^2
AR	1.5
$\Lambda_{c/4}$	38 deg
t/c	8%
λ	0.6
i	0 deg
Γ	34.9 deg
Airfoil	RC-SC2
Ruddervator Span Ratio	63.3%

4.5 Landing Gear Configuration

A retractable, tricycle landing gear configuration was chosen for the Cratus based on flight speeds, necessary drag reduction, and ground handling qualities. This will be discussed further in Chapter 7.

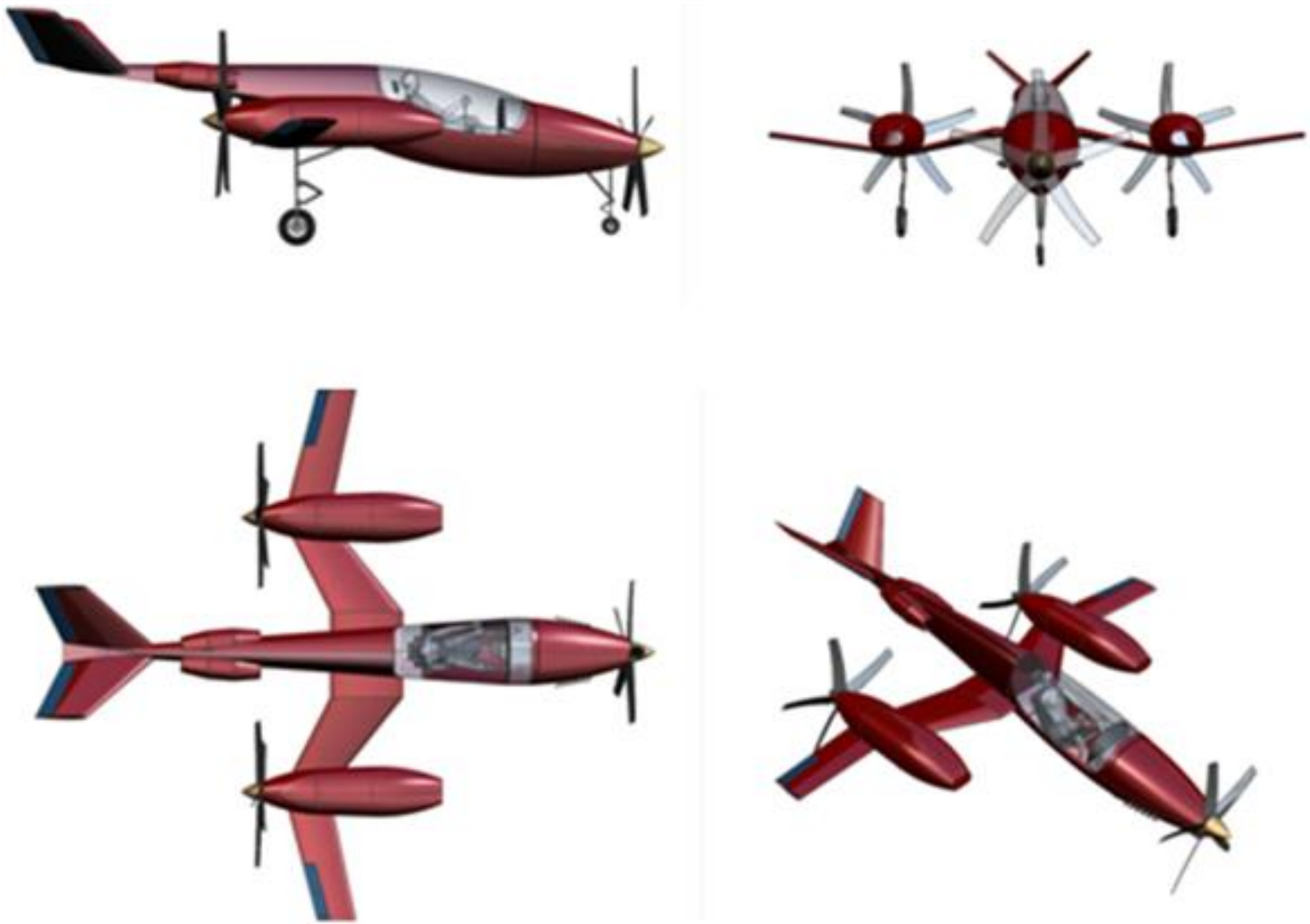

Figure 4.2: Aircraft Three-View and Isometric View (Scale 1:100)

5 Inboard Profile

The cockpit of the Cratus was kept simple. This was to minimize possible error by the pilot during flight. Figure 5.1 shows the cockpit layout.

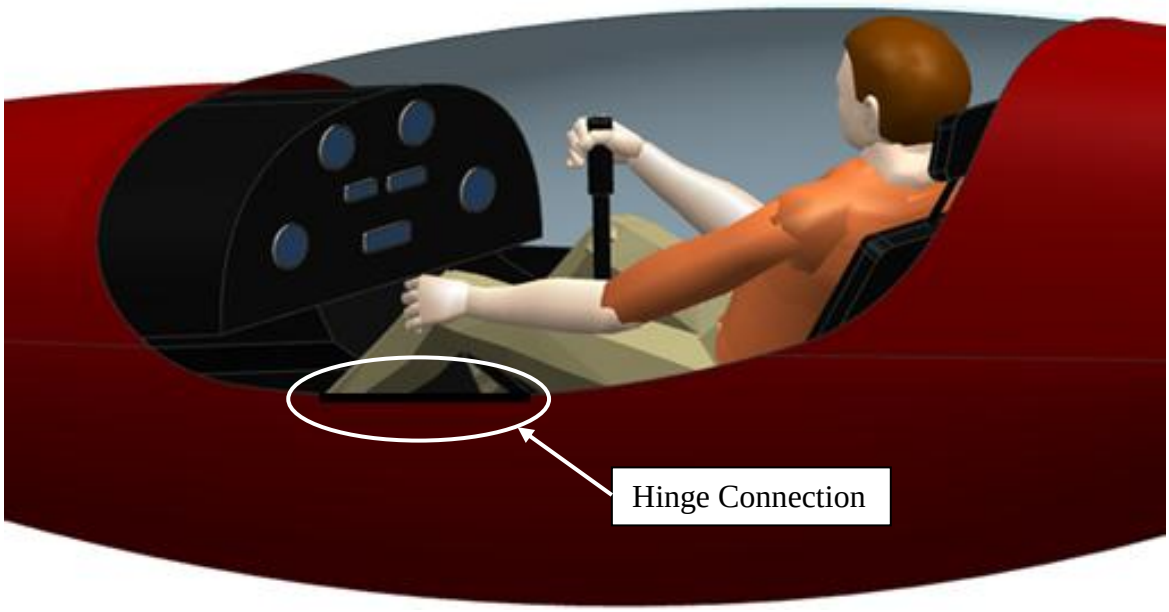

Figure 5.1: Cockpit View

It can be seen from Figure 5.1 that the pilot has ample visibility, especially to the right and left for pilot safety and performance. Ensuring sufficient visibility allows for satisfactory pilot awareness of the aircraft surroundings, including both close flying aircraft and pylons during turning maneuvers. This will improve the performance of the aircraft during the race.

Also seen in Figure 5.1, is the side-hinged canopy. A side-hinge design was implemented for pilot safety. In the event that the pilot needs to evacuate the cockpit immediately upon landing, the hinge pin can be pulled by the pilot and the entire canopy pushed off. This will both evacuate the cockpit air supply if the fire extinguisher is used, as well as allow the pilot an easy exit from the cockpit in any direction.

Figure 5.2 shows a side-view of the cockpit with the 18.3° forward visibility angle. This surpasses the 15° minimum recommended visibility angle.

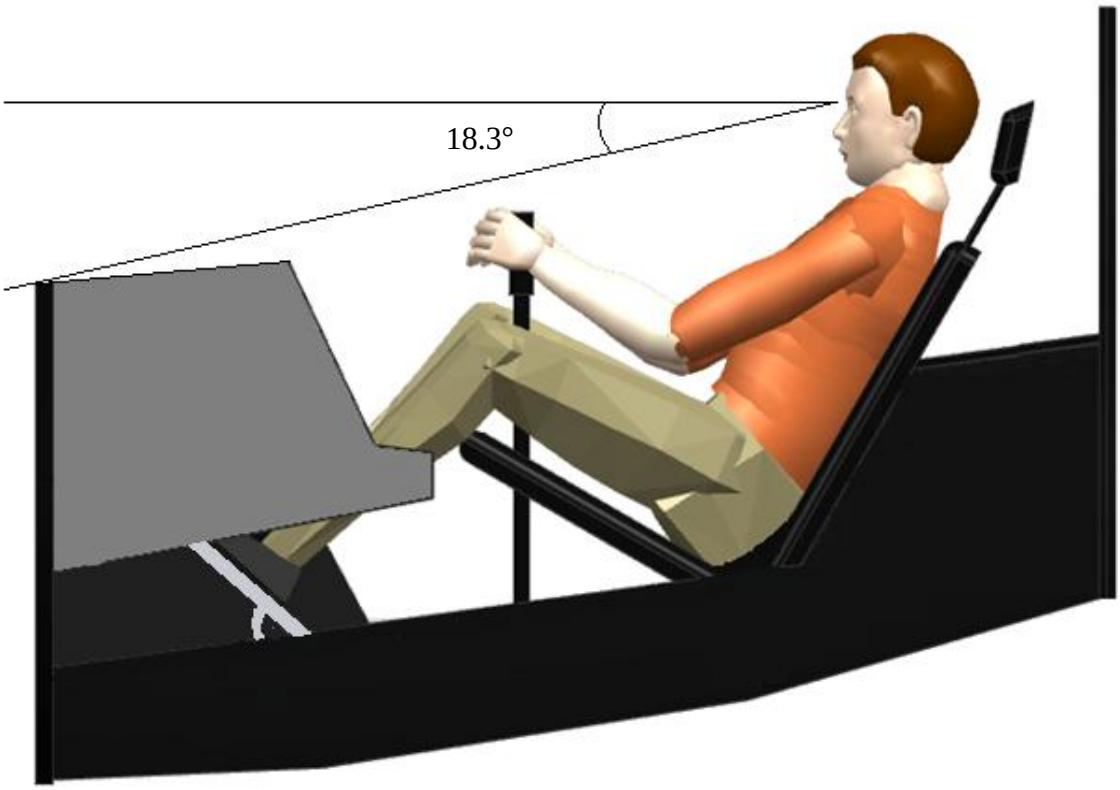

Figure 5.2: Cockpit Side-View

6 Weight Breakdown and CG Excursion Diagram

The weights of the various items within the Cratus were split into three categories: structure, propulsion, and fixed equipment. The items included in each of these categories are listed below:

- Structure: wing, empennage, fuselage, nacelles, landing gear
- Propulsion: power plants, propellers, fuel system, propulsion system, and water injection system
- Fixed Equipment: flight control system, hydraulic system, electrical system, instrumentation/avionics/electronics, auxiliary power unit, and furnishings

The equations used to calculate the weights of the items within the structure category are shown below:

Wing:

$$W_W = 3.08\left[\frac{K_w n_{ult} W_{TO}}{\left(\frac{t}{c}\right)_m}\left\{\left(tan\Lambda_{LE} - \frac{2(1-\lambda)}{A(1+\lambda)}\right)^2 + 1\right\}10^{-6}\right]^{0.593}\{A(1+\lambda)\}^{0.89}(S)^{0.741}$$

(Eq. 5.9, Ref. 10) **Equation 6.1**

Empennage:

$$W_{emp} = 0.04\{n_{ult}(S_v + S_h)^2\}^{0.75}$$

(Eq. 5.16, Ref. 10) **Equation 6.2**

Fuselage:

$$W_f = 11.03(K_{inl})^{1.23}\left(\frac{\bar{q}_L}{100}\right)^{0.245}\left(\frac{W_{TO}}{1{,}000}\right)^{0.98}\left(\frac{l_f}{h_f}\right)^{0.61}$$

(Eq. 5.28, Ref. 10) **Equation 6.3**

Nacelles:

$$W_n = 0.32P_{TO}$$

(Eq. 5.31, Ref. 10) **Equation 6.4**

Landing Gear:

$$W_g = K_{g_r}\{A_g + B_g(W_{TO})^{0.75} + C_g W_{TO} + D_g(W_{TO})^{1.5}\}$$

(Eq. 5.42, Ref. 10) **Equation 6.5**

The propulsion category weight estimates were made using the following equations:

Power plant:

$$W_{pwr} = K_{pg}(W_e + 0.24P_{TO})$$

(Eq. 6.4, Ref. 10) **Equation 6.6**

Propellers:

$$W_{prop} = K_{prop2}(N_p)^{0.218}\{D_p P_{TO}(N_{bl})^{0.5}\}^{0.782}$$

(Eq. 6.14, Ref. 10) **Equation 6.7**

Fuel System:

$$W_{fs} = 2.49\left[\left(\frac{W_F}{K_{fsp}}\right)^{0.6}\left\{\frac{1}{1+int}\right\}^{0.3}(N_t)^{0.20}(N_e)^{0.13}\right]^{1.21}$$

(Eq. 6.17, Ref. 10) **Equation 6.8**

Propulsion System:

$$W_p = W_{ec} + W_{ess} + W_{pc} + W_{osc}$$

(Eq. 6.27, Ref. 10) **Equation 6.9**

$$W_{ec} = 60.27\left\{\frac{(l_f + b)N_e}{100}\right\}^{0.724}$$

(Eq. 6.31, Ref. 10) **Equation 6.10**

$$W_{ess} = 50.38\left(\frac{W_e}{1{,}000}\right)^{0.459}$$

(Eq. 6.36, Ref. 10) **Equation 6.11**

$$W_{pc} = 4.552(N_{bl})^{0.379}\left\{\frac{N_p D_p P_{TO}}{1{,}000}\right\}^{0.759}$$

(Eq. 6.38, Ref. 10) **Equation 6.12**

$$W_{osc} = K_{osc} W_e$$

(Eq. 6.43, Ref. 10) **Equation 6.13**

Water Injection System:

$$W_{wi} = \frac{8.586 W_{wtr}}{8.35}$$

(Eq. 6.42, Ref. 10) **Equation 6.14**

The weight estimates for the fixed equipment were made using the following equations:

Flight Control System:

$$W_{fc} = 23.77\left(\frac{W_{TO}}{1{,}000}\right)^{1.1}$$

(Eq. 7.11, Ref. 10) **Equation 6.15**

Hydraulic System:

$$W_{hps} = 0.005 W_{TO}$$

(Page 101, Ref. 10) **Equation 6.16**

Electrical System:

$$W_{els} = 0.0268 W_{TO}$$

(Eq. 7.13, Ref. 10) **Equation 6.17**

Instrumentation, avionics, and electronics:

$$W_{iae} = 40 + 0.008W_{TO}$$

(Eq. 7.23, Ref. 10) **Equation 6.18**

Auxiliary Power Unit:

$$W_{apu} = 0.004W_{TO}$$

(Eq. 7.40, Ref. 10) **Equation 6.19**

Furnishings:

$$W_{fur} = 0.412\left(N_{pax}\right)^{1.145}(W_{TO})^{0.489}$$

(Eq. 7.41, Ref. 10) **Equation 6.20**

The values found from the above calculations are shown in Table 6.1; the fuel, cooling water, and pilot weights are also included. For each item, the location of the center of gravity is estimated, seen in Table 6.1, to find the center of gravity excursion for the aircraft in different flight conditions.

Table 6.1: Component Weights and CG Locations

Component	Weight (lbf)	CG FS (in)
Wing	185.19	76
Empennage	17.17785	147
Fuselage	146.42	47
Nacelles (2)	592.64	68
Landing Gear	375.5307	52
Power Plants (3)	1,305.1	54
Propellers (3)	291.1228	57
Fuel System	38.90062	67
Propulsion System	179.2971	59
Water Injection System	1044.716	58
Fixed Equipment	531.9357	55
Fuel	524	56
Water	1,016	53
Pilot	150	55

Figure 6.1 shows the CG location of each component on the aircraft.

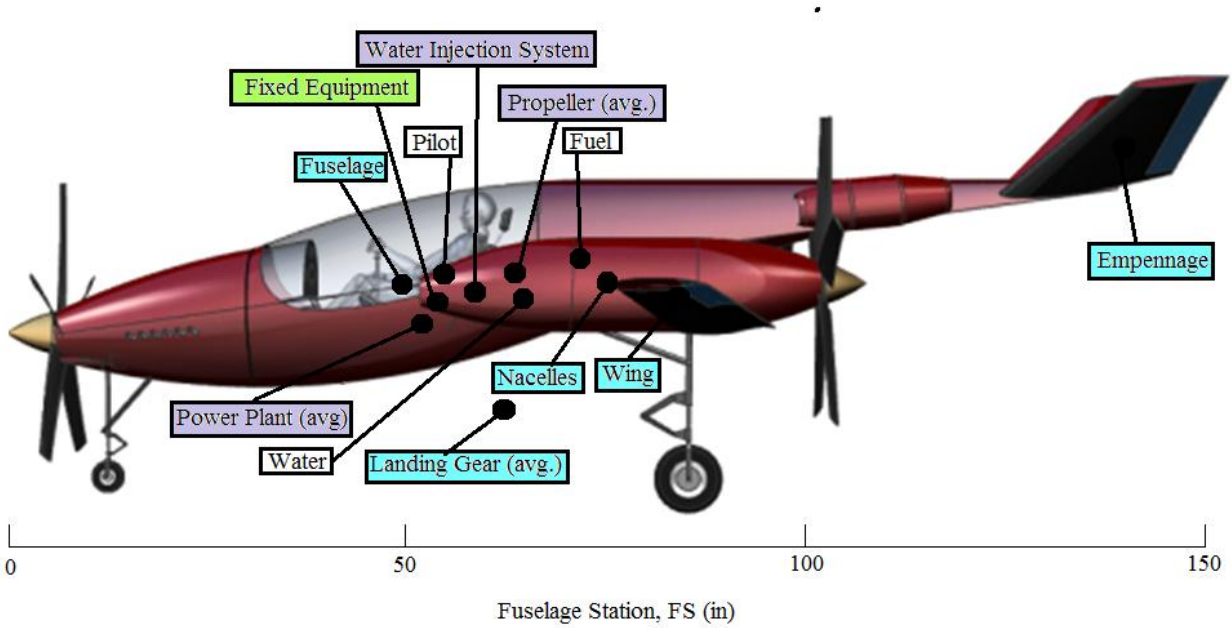

Figure 6.1: Component CG Locations

The fuel and water are variable weights which contribute to the CG excursion of the aircraft. Iterations were performed to locate the aircraft components in a manner which resulted in an acceptable CG excursion. The CG excursion graph is shown in Figure 6.2.

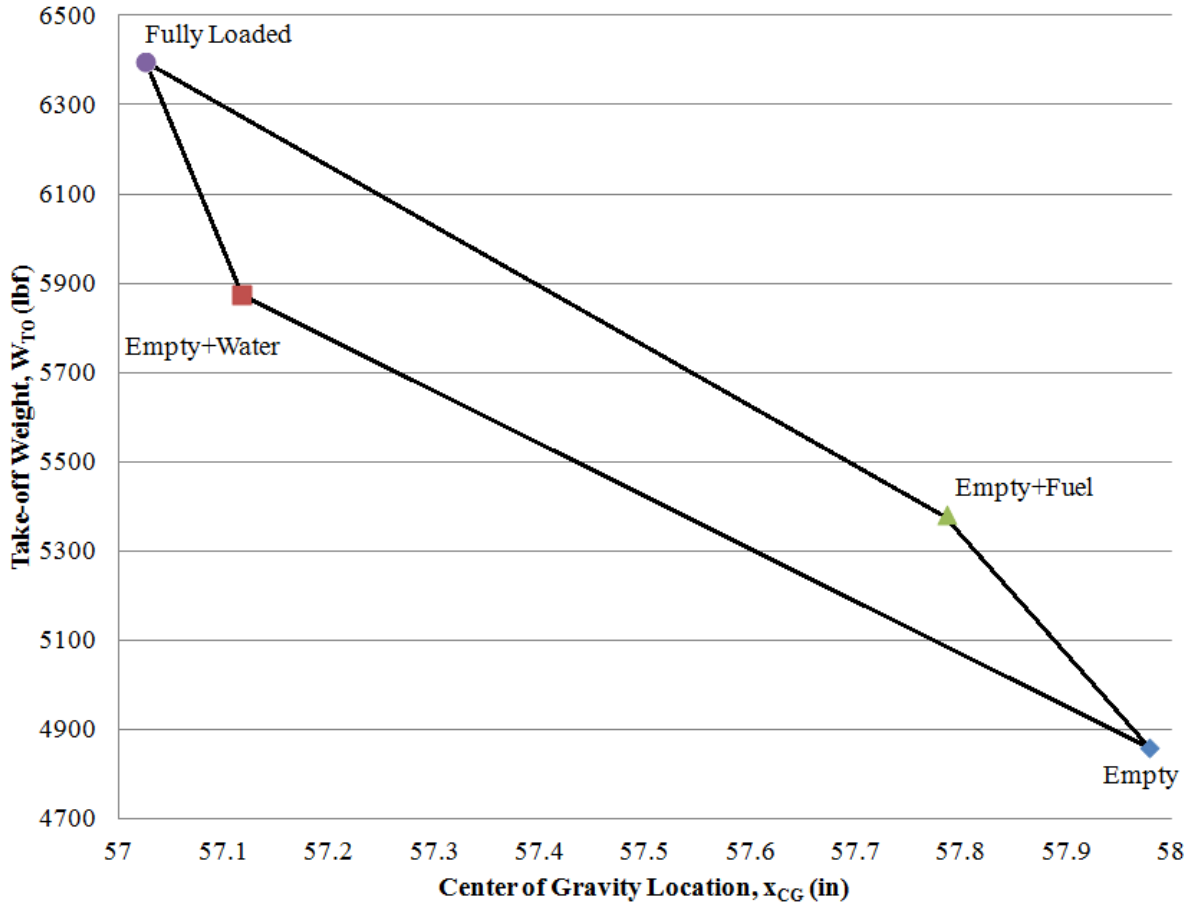

Figure 6.2: CG Excursion Diagram

Figure 6.2 shows that the CG excursion for the Cratus is acceptable with less than 1 inch excursion. This CG shift prevents aircraft instability during flight when fuel is burned and water is used for engine cooling. The justification for minimizing the CG excursion beyond a typical 10% is for uncertainties. It is likely that the pilot will not weigh exactly 150 lbf, therefore the added or reduced weight of the pilot will not shift the CG beyond an acceptable range.

7 Sizing of Landing Gear

Retractable, tricycle landing gear was chosen for the Cratus. Retractable gear was an obvious choice considering the significant drag which would be experienced by the aircraft if fixed gear were used, thus decreasing the performance of the aircraft considerably. Tricycle gear was preferred due to pilot visibility during taxi, take-off, and landing, ground handling, and take-off rotation.

7.1 Tire and Strut Sizing

Proper sizing of the strut and tires requires the calculation of the static load which will act on each strut. This was done using the following equations:

$$P_n = \frac{W_{TO} l_m}{l_m + l_n}$$

(Eq. 9.1, Ref. 11) **Equation 7.1**

$$P_m = \frac{W_{TO} l_n}{n_s (l_m + l_n)}$$

(Eq. 9.2, Ref. 11) **Equation 7.2**

Type VII tires were chosen for their performance on runways with rigid pavement. Type VII tires also have a high load capacity as well as narrow widths. The tire sizes were determined by the predicted static and dynamic loads. Static loads were used for the main gear, while dynamic loads were used for the nose gear to account for hard landings. The calculated loads are shown in Table 7.1.

Table 7.1: Landing Gear Loads

Nose Gear	Load
Maximum Static Load	674 lbf
Maximum Dynamic Load	1,012 lbf
Main Gear	
Maximum Static Load	2,861 lbf

Following Reference 11 and the calculated loads listed in Table 7.1, the following tires were chosen for the Cratus:

- Nose Gear: $D_t x b_t$=7”x2.5” with 40 psi
- Main Gear: $D_t x b_t$ =10”x4.5” with 60 psi

7.2 Strut and Shock Absorber Sizing

The shock absorber length and diameter were calculated using the following equations:

$$s_s = \frac{\frac{0.5\left(\frac{W_L}{g}\right)w_t^2}{n_s P_m N_g} - \eta_t s_t}{\eta_s}$$

(Eq. 2.11, Ref. 11) **Equation 7.3**

$$d_s = 0.041 + 0.0025(P_m)^{0.5}$$

(Eq. 2.13, Ref. 11) **Equation 7.4**

Table 7.2: Shock Absorber Dimensions

Nose Gear Shock Absorber	Value
Stroke	4.72 in
Diameter	1.6 in
Main Gear Shock Absorber	
Stroke	9.63 in
Diameter	2.2 in

The values found for the shock absorbers stroke and diameter for both the nose and main gear are listed in Table 7.2.

7.3 Landing Gear Location

The following criteria were considered when locating and designing the landing gear: longitudinal tip-over, longitudinal ground clearance, and lateral ground clearance. Figure 7.1 and 7.2 show that the Cratus satisfies the criteria listed above.

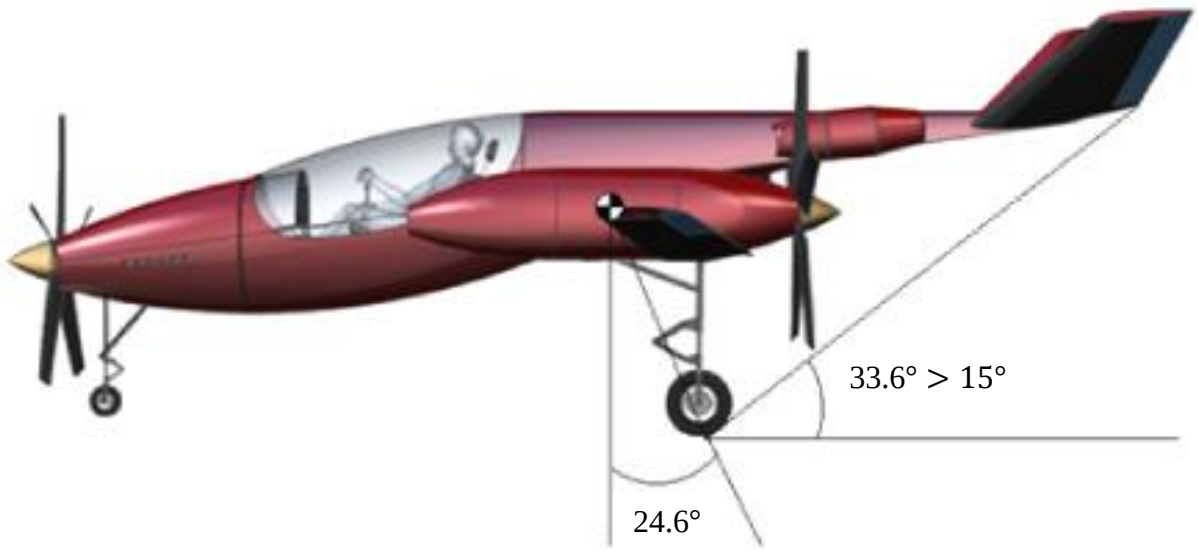

Figure 7.1: Longitudinal Ground Clearance and Tip-Over

Figure 7.2: Ground Clearance

8 Drag Build-Ups and Drag Polars

8.1 Zero-Lift Drag Coefficients

The zero-lift drag coefficient for the wing, fuselage, empennage, and nacelles of the aircraft were calculated using the following equations, respectively:

$$C_{D_{o_w}} = (R_{wf})(R_{LS})(C_{f_w})\{1 + L'(t/c) + 100(t/c)^4\}\frac{S_{wet_w}}{S} + C_{D_{wave}}$$

(Eq. 4.6, Ref. 12) **Equation 8.1**

$$C_{D_{o_{fus}}} = (R_{wf})\left(C_{f_{fus}}\right)\left\{1 + 60/\left(l_f/d_f\right)^3 + 0.0025\left(l_f/d_f\right)\right\}\frac{S_{wet_{fus}}}{S} + C_{D_{b_{fus}}}$$

(Eq. 4.30, Ref. 12) **Equation 8.2**

$$C_{D_{o_{emp}}} = (R_{wf})(R_{LS})(C_{f_w})\{1 + L'(t/c) + 100(t/c)^4\}\frac{S_{wet_{emp}}}{S} + C_{D_{wave}}$$

(Eq. 4.6, Ref. 12) **Equation 8.3**

$$C_{D_{n_{int}}} = 0.036\left(\frac{c_n b_n}{S}\right)\left(\Delta c_{l_1} + \Delta c_{l_2}\right)^2 \ (nacelle - wing\ interference)$$

(Eq. 4.63, Ref. 12) **Equation 8.4**

$$\Delta C_{D_{wmprop}} = \frac{33(1/\bar{q}S)SHP_{rated}}{V_1} \ (windmilling\ drag)$$

(Eq. 4.68, Ref. 12) **Equation 8.5**

Considering the speeds that the Cratus will be flying, compressibility effects must be considered. These are important to include in the calculation of drag for the wing and empennage of the Cratus because compressibility effects are strongly affected by the thickness ratio (mainly lifting surfaces). The additional drag due to these effects was found using Figure 2.3 from Reference 12.

Table 8.1: Component Zero-Lift Drag Coefficients

Component	Zero-Lift Drag Coefficient
Wing	0.00837
Fuselage	0.00755
Empennage	0.00188
Nacelles	0.00962
Landing Gear	0.02087

The landing gear drag coefficient was estimated through the calculation of the tire reference area and the use of Figures 4.58 and 4.59 in Reference 12 for the nose gear and main gear, respectively. The values found for the nose gear and main gear drag coefficients were then added together to find the total landing gear drag coefficient. The values found from the above calculations are listed in Table 8.1.

8.2 Drag Polars

The drag polars were graphed using the following equation:

$$D = \frac{1}{2}\rho V^2 S C_{D_o} + \frac{2n^2 W^2}{\rho V^2 S \pi A e}$$

(Eq. 2.4, Ref. 12) **Equation 8.6**

A drag polar was created for the cruise, take-off, and landing flight segments since these are the most drag sensitive. The source of variation between the three segments is significant due to the differences in flight speed and G-loading.

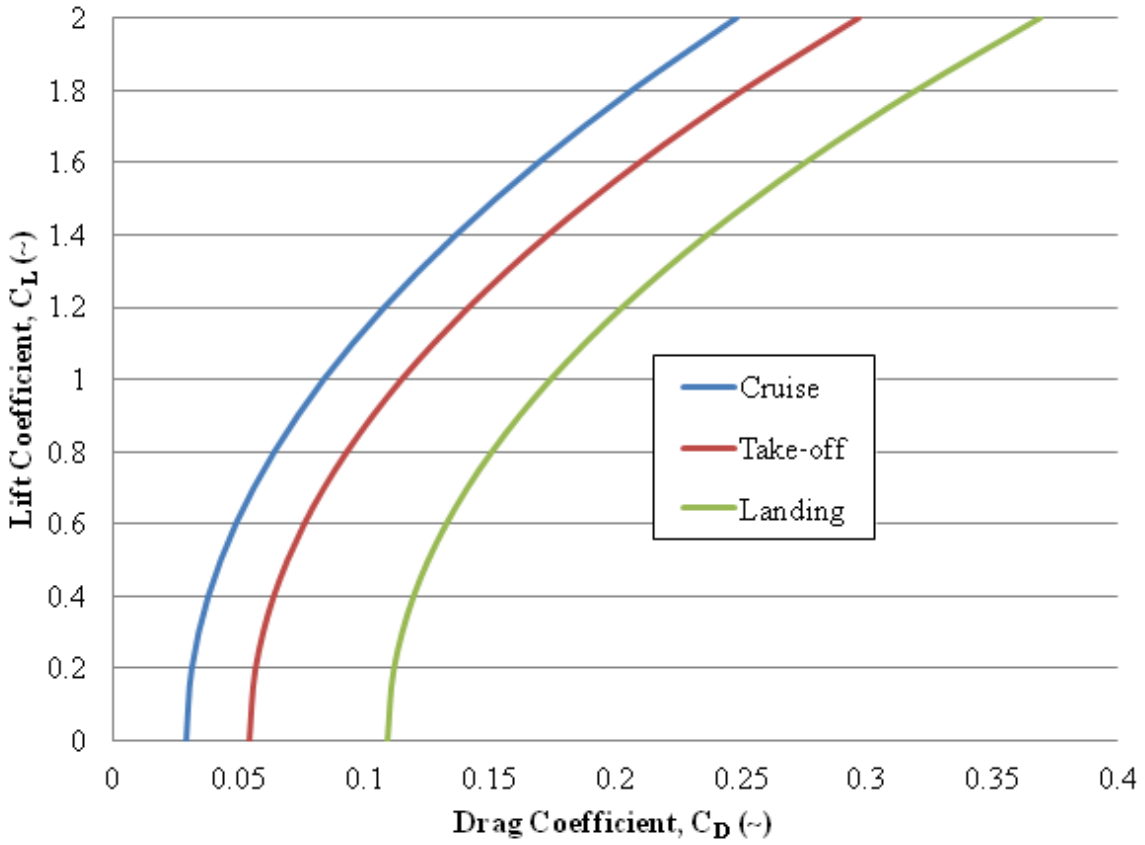

Figure 8.1: Drag Polars at Cruise, Takeoff, and Landing

9 Class II Propulsion Performance

The BMW P84 V10 engine was chosen for use on the Cratus. An image of the engine can be seen below in Figure 8.1 along with the general characteristics listed in Table 9.1 (Ref. 13).

Table 9.1: Engine Characteristics

Characteristic	Value
P	926 hp
W	203 lbf
h	12.6 in
w	21.1 in
l	22.8 in

Figure 9.1: BMW P84 V10 Engine[13]

Due to the transonic speeds seen by the aircraft during race conditions, a propfan will be used. This increases the performance of the aircraft through increased propulsion efficiency at transonic flight speeds. The figure below shows propeller efficiency trends for advanced propfans according to Reference 14.

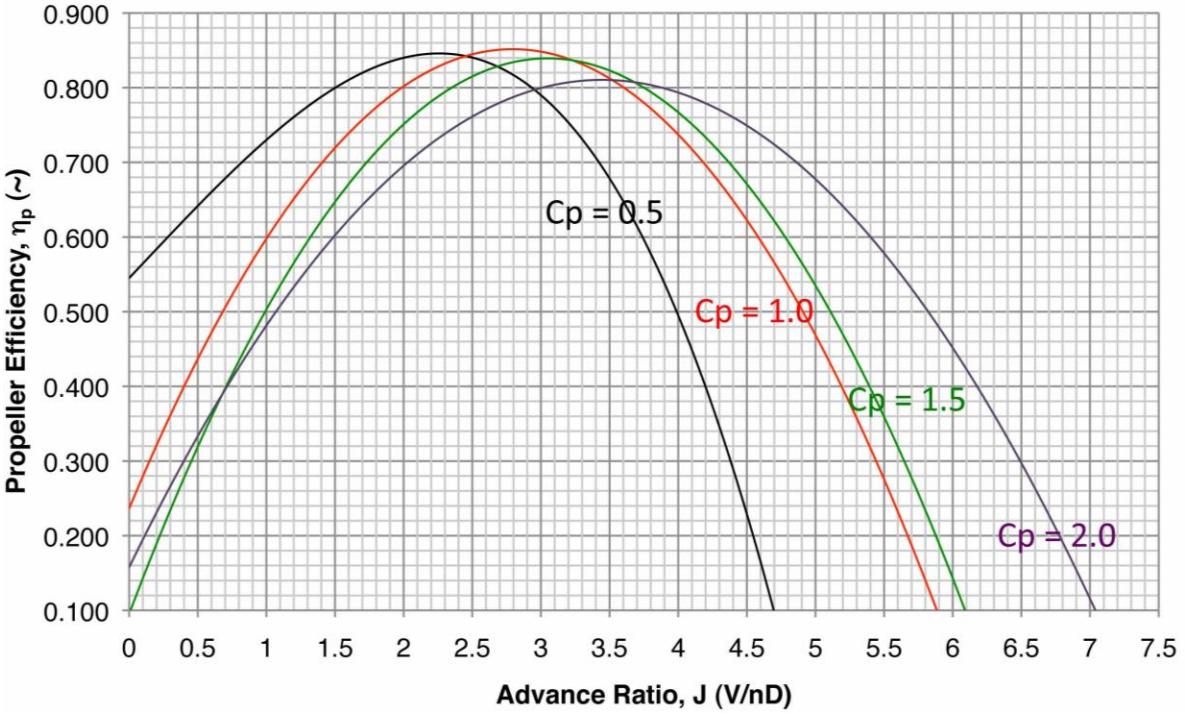

Figure 9.2: Propfan Performance

If the tip speed of the propeller is constrained to Mach 0.95 during full power of 926 hp, the following correlation, shown in Figure 9.3, can be seen between advance ratio and power coefficient with respect to airspeed for an advanced propfan.

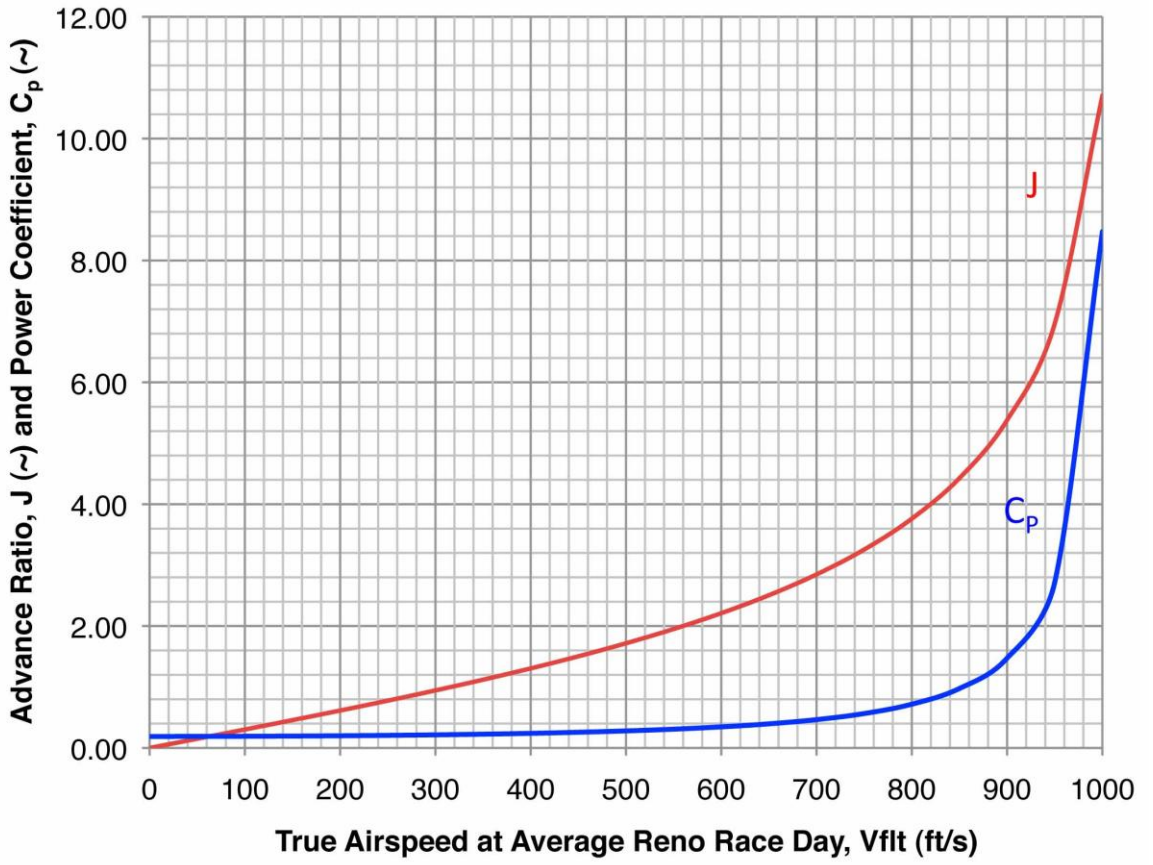

Figure 9.3: Constrained Advance Ratio and Power Coefficient Trends

Assuming typical race day conditions, Figure 9.4 shows the propeller efficiencies which are attainable following the trends shown in Figure 9.3.

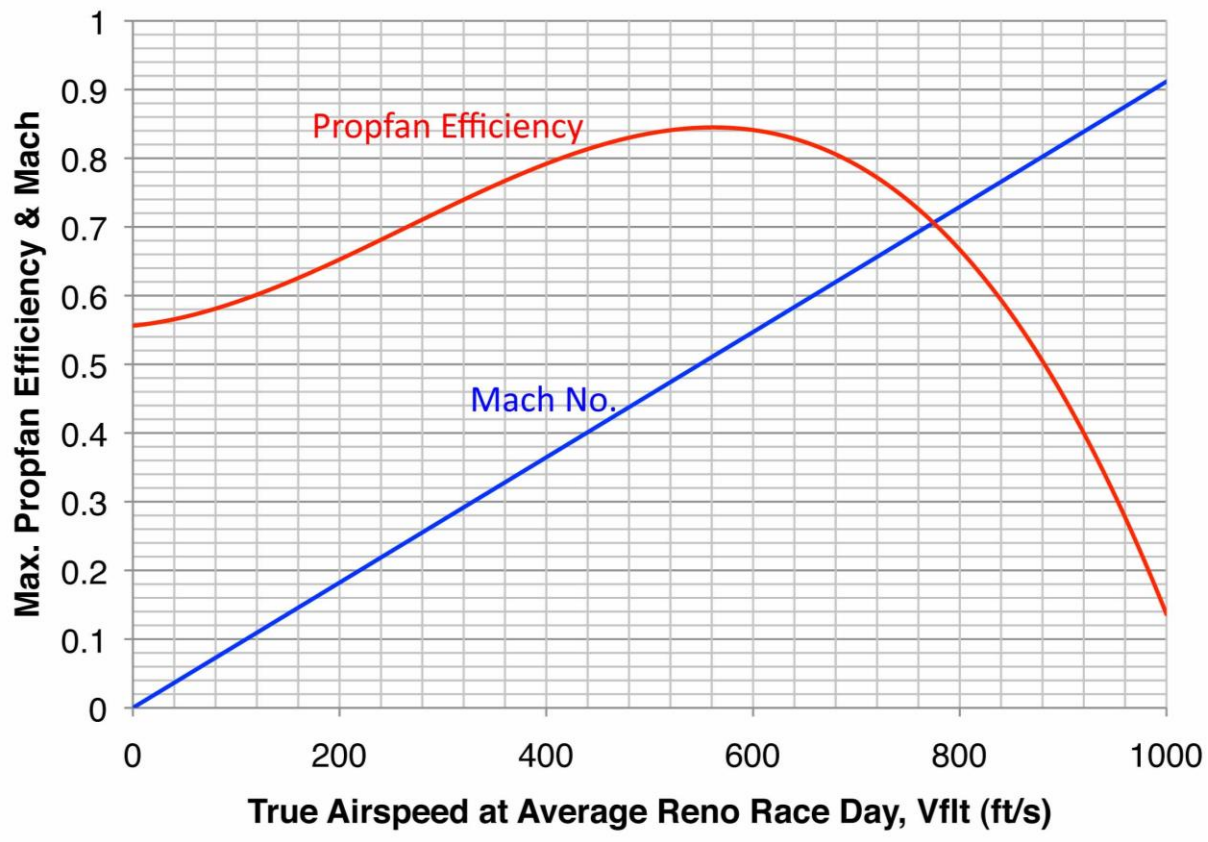

Figure 9.4: Propeller Efficiency

Using the trend lines above, momentum theory, and a Figure of Merit of 0.6 for static thrust, the uninstalled and installed thrust levels of the aircraft were found. This was done using techniques outlined in Reference 15 and are shown below in Figure 9.5.

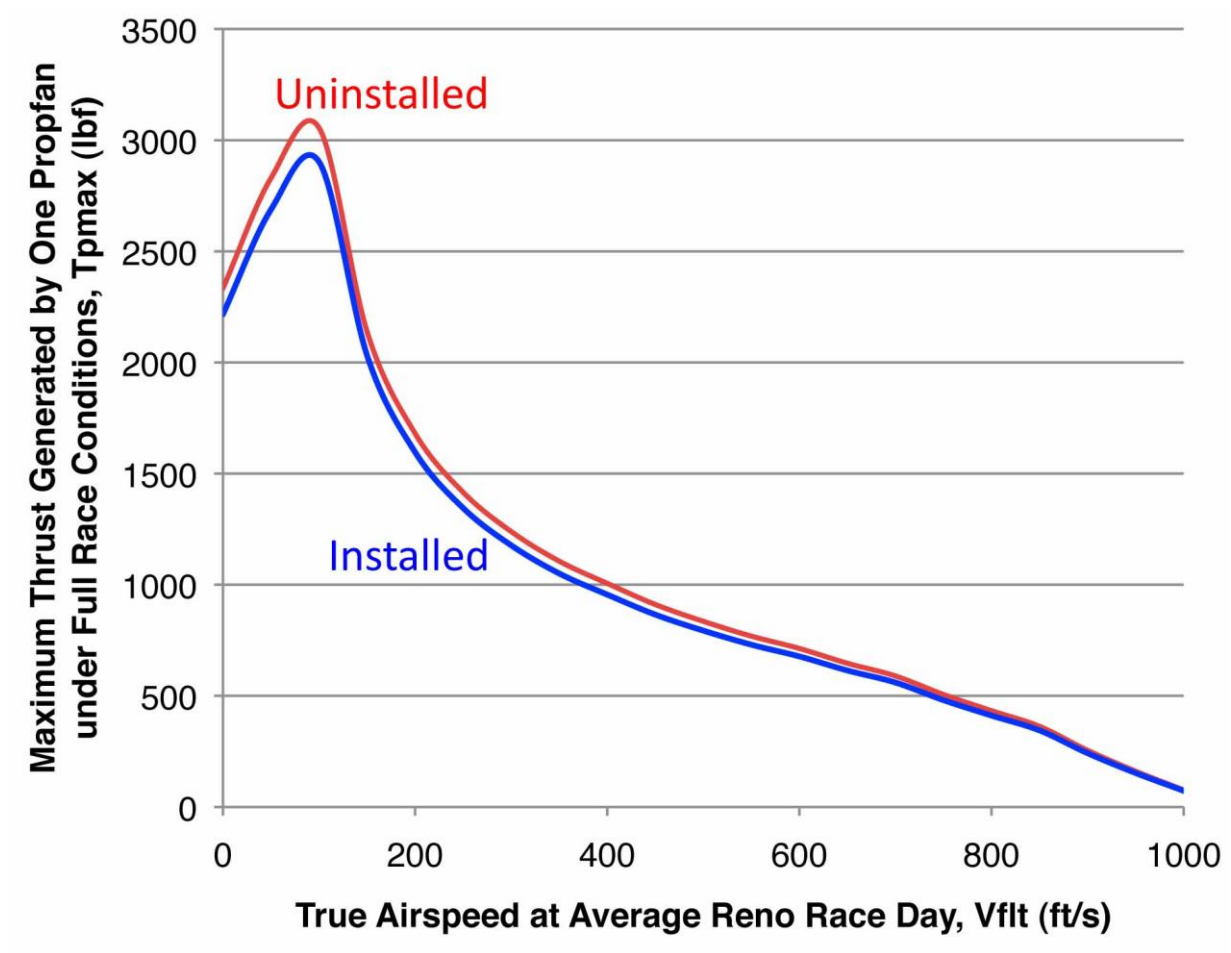

Figure 9.5: Installed and Uninstalled Thrust

9.1 Lost Mass Meredith Effect

Engine cooling is a vital detail for any Reno racer. The Cratus seeks to combine two methods currently used by many racers. These methods include lost mass water cooling and Meredith effect. Meredith effect simply takes advantage of the already present hot air from the radiator and uses it in a Brayton cycle to produce additional thrust for the aircraft. Lost mass cooling uses fluid evaporation, in this case water, to cool the engine. Using both lost mass cooling and Meredith effect, the Cratus will utilize the exhaust gases typically lost with a

standard cooling system. The total chemical power of combustion of a typical racing engine's power flow is shown below:

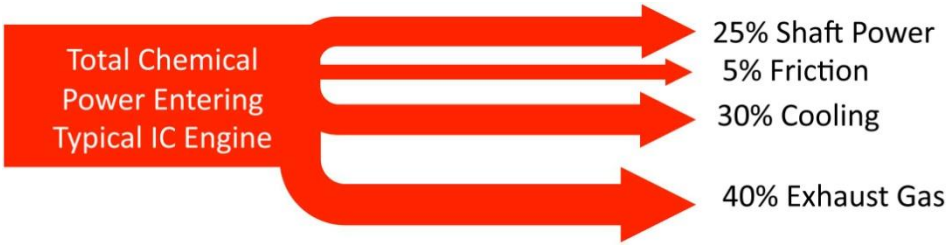

From this, it is seen that roughly 40% of the total chemical power entering the engine is wasted through the exhaust gases leaving the engine.

It is assumed that employing the Meredith effect is an acceptable addition to the aircraft seeing as many P-51s currently racing use this effect, including the Dago Red racer. The use of lost mass cooling stands within the stated rules, therefore it is assumed that combining Meredith effect and lost mass cooling will an acceptable design philosophy. In the event that the judges see this as a misinterpretation of the race rules, the use of Meredith effect will be eliminated and the additional thrust gained by this design will be forfeited. Calculations were completed for the following cases to account for the possibility of not utilizing all effects: Meredith effect and lost mass cooling, Meredith effect thrust addition, and no thrust addition from the radiator.

9.2 Lost Mass Effect

A synthetic oil will be used which will allow the engine to operate with oil temperatures above 400°F. The water which enters the heat exchanger will be roughly 50°F. Upon leaving the heat exchanger, the water will be at its boiling point. It will then be vaporized and continued to be heated to the assumed oil temperature of 400°F. At a temperature of 400°F, the internal energy of the water will reach 1,582 $\frac{hp}{lbm/s}$ (2.6 MJ/kg). The total chemical power

breakdown which was shown above reveals a relationship between cooling losses and shaft power. This relationship shows the requirement of 1.2 hp of cooling per hp of shaft power.

This results in a water mass flow of 0.0456 $\frac{lbm/min}{shp}$ for proper cooling. Therefore, the water consumption rate for three engines is 126.7 lbm/min, or 1,014 lb of water for one race, assuming an 8 minute race.

It is assumed that the steam will be fully heated to 400°F and contained at its full vapor saturation pressure of 265 psi. It will then be expanded to ambient conditions through the use of a convergent-divergent nozzle. This will generate a Mach 2.52 exit velocity. Assuming fully expanded flow, $P_e = P_a$, the following equation was used to calculate the thrust generated by the steam flow.

$$F = \dot{m}V_e + (P_e - P_a)Ae$$

(Ref. 16) **Equation 9.1**

This results in an added thrust of 211 lbf with all engines operable.

9.3 Effects of Lost Mass and Meredith Effect

It is assumed from Reference 17, that including Meredith effect will increase thrust an additional 80% beyond lost mass cooling. Therefore the total additional thrust from cooling will be 380 lbf, assuming all methods are accepted. Figure 9.7 shows the total thrust available when all three engines are operable.

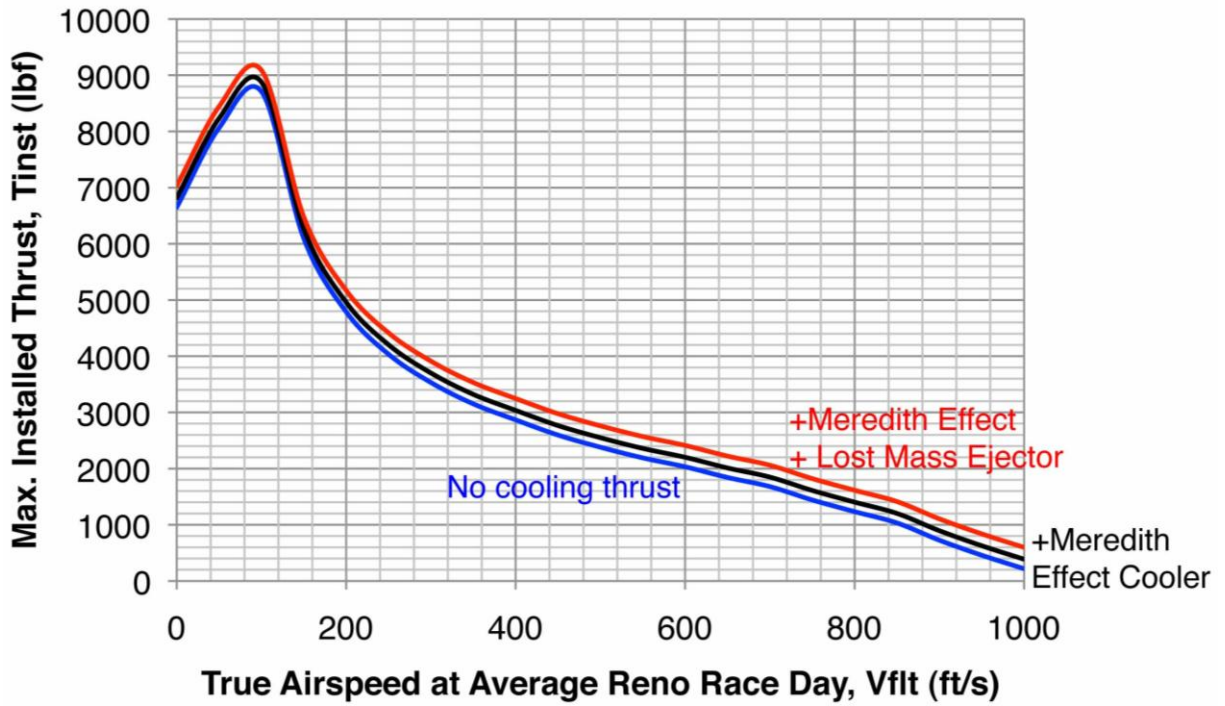

Figure 9.6: Available Thrust

Combining the available thrust with the drag found for the aircraft yields Figure 9.7.

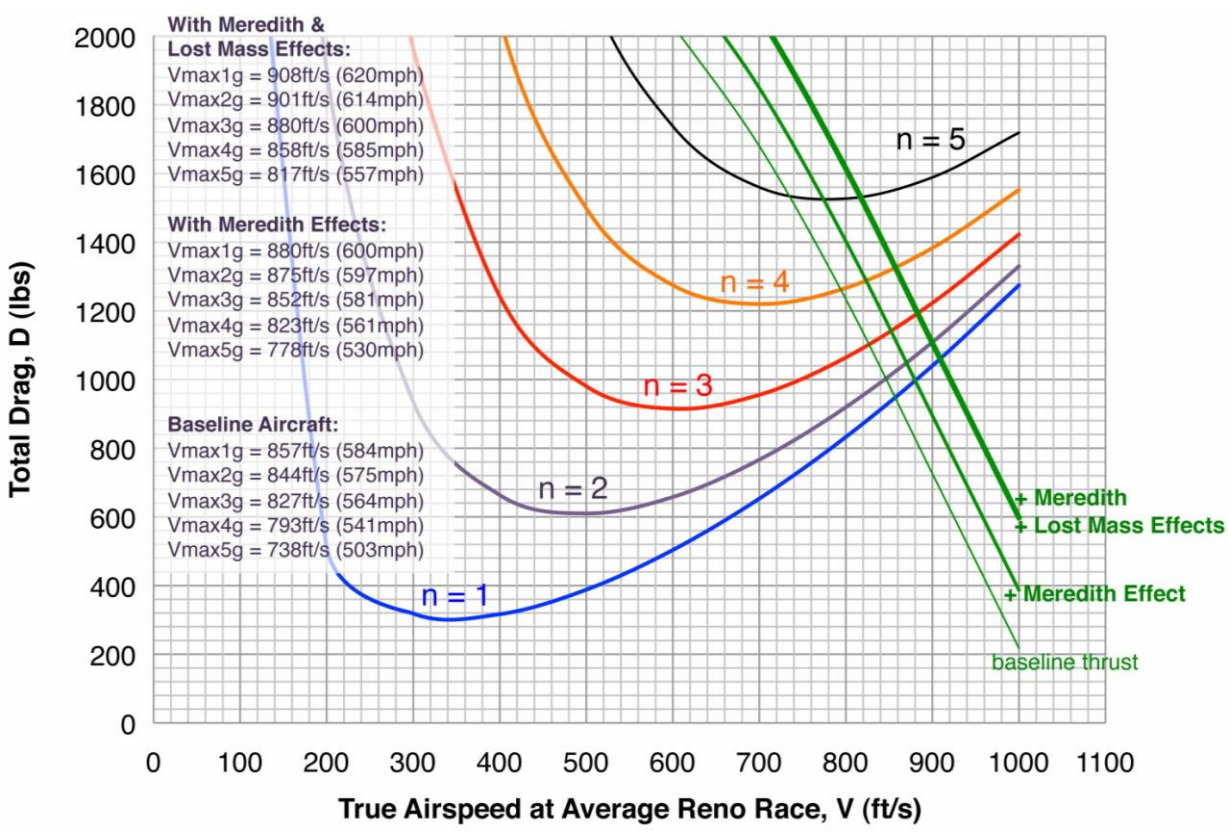

Figure 9.7: Attainable Flight Speeds

It is possible to calculate the nominal accelerations as a function of radii of the vertices of the flight path around the race course. The largest accelerations are experienced at the smallest radii turns; therefore these turns were used as the flight speed limiting factor. Various flight paths were created with different turn radii to compare flight speeds. These flight paths are shown in Figure 9.8.

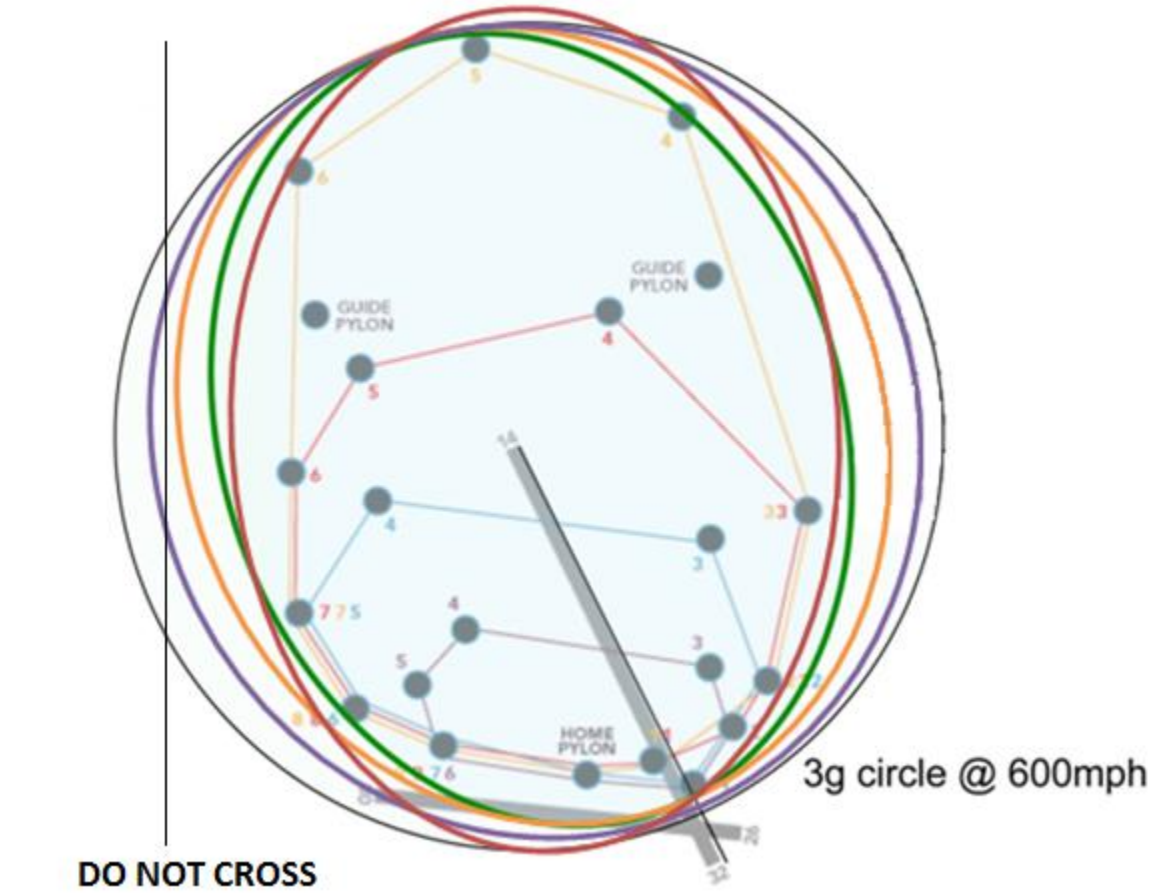

Figure 9.8: Race Course and Flight Paths

As is seen in Figure 9.8, the line which designates the edge of the race field limits the width of the flight path. Considering this and the flight path rules of the races, the flight path which optimizes the speed of the aircraft over the full course of the race was found to be the green circle shown in Figure 9.8. Overlaying the average centripetal acceleration from the optimized flight path with respect to aircraft speed and the thrust available curves results in the following maximum flight speeds, shown in Figure 9.9.

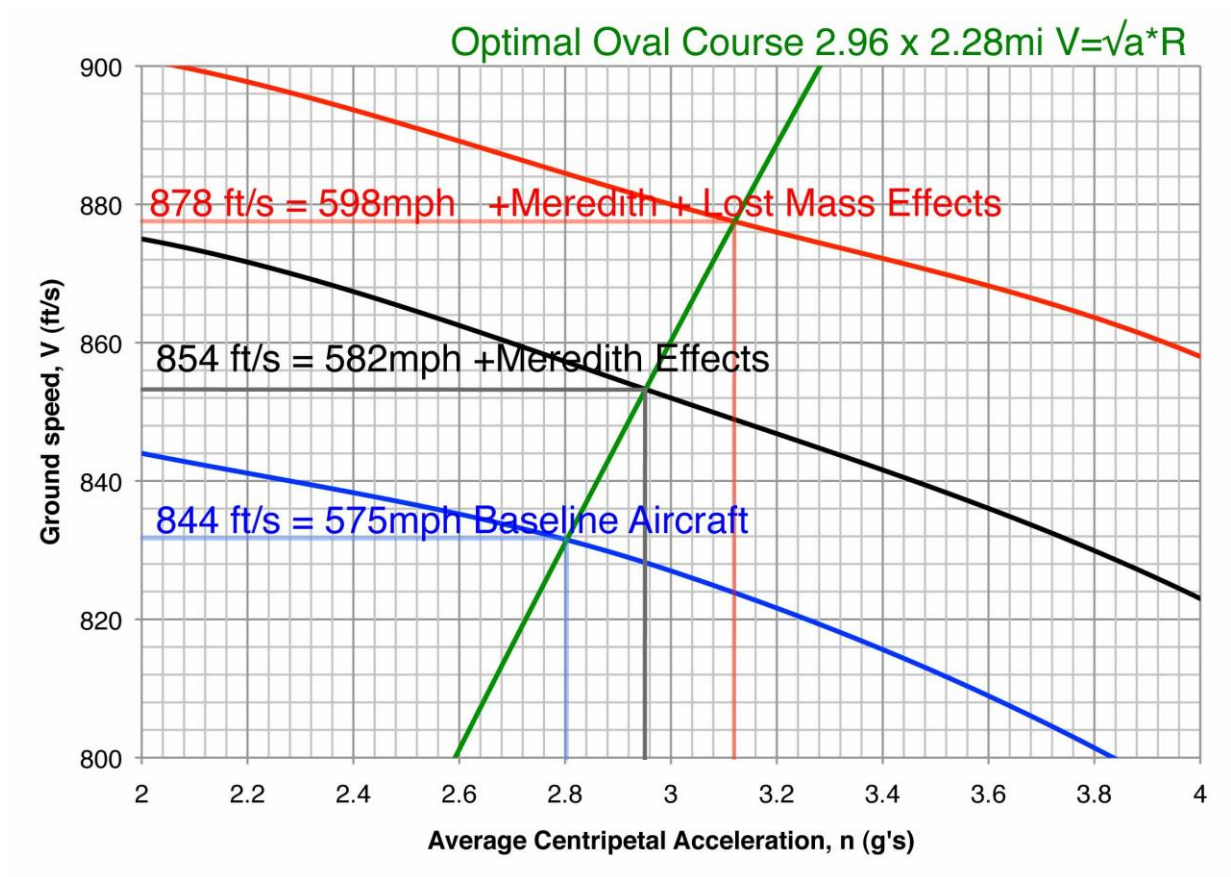

Figure 9.9: Attainable Course Lap Speeds

From Figure 9.9, the maximum average course speed which can be attained with Meredith effect and loss mass is 598 mph. If these methods are not allowed, the maximum average course speed is 575 mph. This shows that the Cratus is able to easily beat the record holding times with or without the thrust generating radiators.

10 Stability and Control

10.1 Longitudinal Stability

It was determined that positive-inherent stability was important for the Cratus. This was chosen for reliability in the event of systems failure, disturbances, and engine failure. The risk of complete aircraft destruction in the event of systems failure is lessened with positive inherent stability.

The static margin of the Cratus was chosen to be around 3%. This ensures that the benefits of an inherently stable aircraft are attained, but a value less than 10% decreases the stability of the aircraft, thereby increasing the maneuverability. A static margin of 3% will still allow enough time for the pilot to safely react to fly the aircraft.

The x-plot, created following the procedure in Reference 18, is shown below in Figure 10.1.

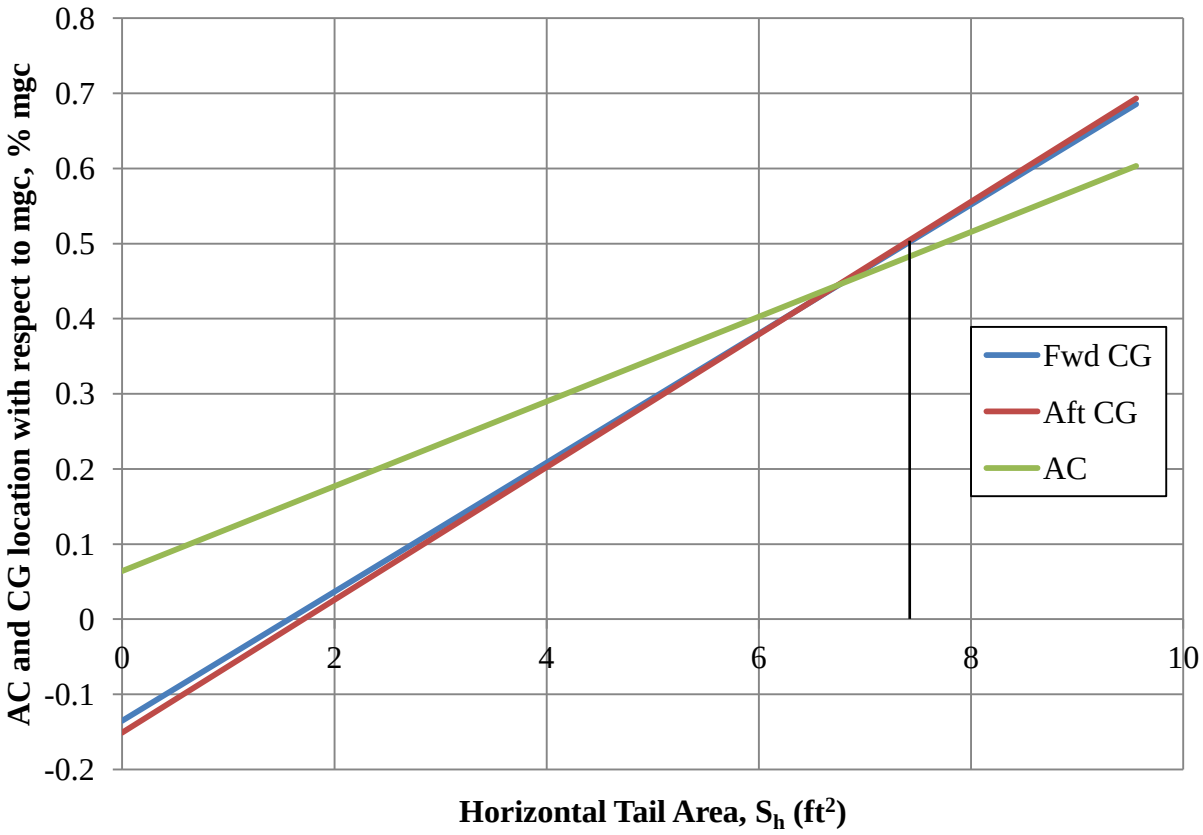

Figure 10.1: Longitudinal X-Plot

From Figure 10.1, the horizontal tail area was chosen as 7.6 ft^2. This results in a static margin of 2.92% and a maximum static margin of 3.23%. The center of gravity travel is 0.31%.

10.2 Directional Stability

The directional x-plot, shown below in Figure 10.2 and created following the procedure in Reference 18, was used to determine an acceptable vertical tail area.

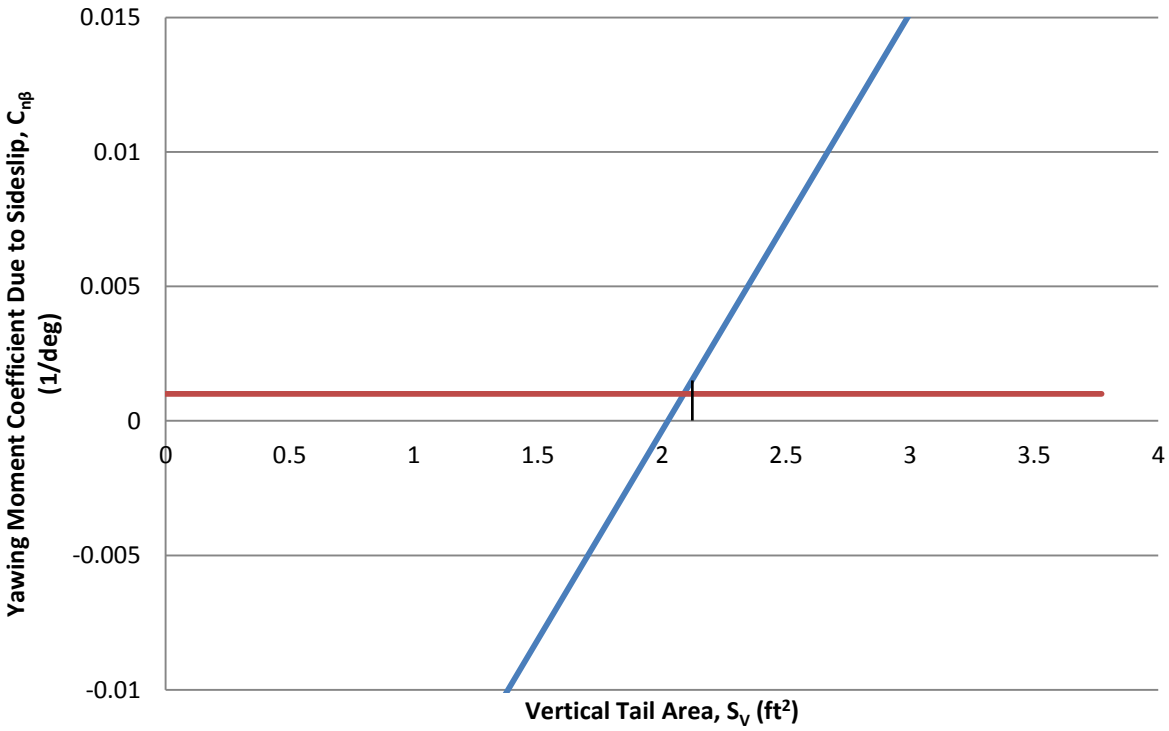

Figure 10.2: Directional X-Plot

According to Reference 18, an acceptable yawing moment coefficient due to sideslip is 0.001/deg. From Figure 10.2, it can be seen that an acceptable vertical tail area is 2.1 ft^2.

10.3 V-Tail Construction

A v-tail empennage was chosen for the Cratus due to the wetted area and weight it would save as compared to a conventional tail. A v-tail also provides less complex flight control systems because only two control surfaces need to be controlled as opposed to three or more. With respect to a Reno racer with laterally displaced engines, a v-tail is ideal because the shape prevents the tail from being completely located within the prop wash. The shape also prevents

the equivalent horizontal tail area from becoming blanked by the fuselage during maneuvers and high angle of attack flight. The empennage drag is reduced not only by the reduction in wetted area, but also interference drag. There is only one connection angle on a v-tail; therefore the interference drag is reduced in comparison to a conventional tail which has two connection angles.

The size of the horizontal and vertical tail as was found in Sections 10.1 and 10.2 were scaled using a $\sqrt{2}$ sizing ratio to find the equivalent area of the v-tail. This prevents over-sizing of the empennage. The resulting v-tail area is 5.58 ft^2, 2.79 ft^2 for each surface. To satisfy the stability stated in Sections 10.1 and 10.2 with a 3% static margin, the two surfaces will be at an angle of 38.4° from the horizontal plane of the fuselage-empennage intersection.

10.4 One Engine Inoperative

The low flight altitudes at which the Reno Races take place make it very dangerous for pilots flying multi-engine aircraft. This is due to the yawing moment experienced if one engine becomes inoperable. The low altitudes cause the time from engine failure to ground impact to be faster than the pilot and aircraft reaction time to regain control of the aircraft. To avoid this problem, the wing engines in the Cratus contain an electrical feathering system. In the event that one engine's thrust output equals zero, both wing engine propellers will automatically feather. This will decrease the propeller drag considerably and minimize the unsymmetrical power output which would otherwise be experienced.

11 Structure

11.1 Fuselage Structure

The fuselage of the Cratus will be constructed of AS4/MTM 45-1 carbon/epoxy cloth composite and TI-6Al-4V reinforcements including ring frames, bulkheads, keel beams, and ribs. The carbon composite skin will contain a layer of 1 inch honeycomb between the outer and inner surfaces to assist in supporting compressive loads acting on the aircraft.

For increased visibility the canopy will be high strength polycarbonate with titanium connection points. These materials have proven effective in various aerospace application including the Piaggio P-180 and F-22 Raptor.

Carbon fiber composite was chosen for the fuselage because of its ability to form complex mold lines. Its high specific strength reduces the weight while also giving the structure the required strength to withstand the high loads it will encounter.

Using a composite for the skin of the aircraft results in a lower friction drag compared to a traditional aluminum skin. With a metal skin, joints are required due to manufacturing and material limitations. A composite structure allows for joints to be built within the surface, resulting in a smoother aerodynamic surface leading to a reduction in friction drag.

Cloth composite will be used due to its high damage tolerance as compared to other composite types such as tape. Damage tolerance is an important aspect for a Reno Racing structure because of the sandy environment. The high damage tolerance of the cloth composite will allow the low drag, aerodynamic surfaces of the aircraft to be maintained.

Titanium was chosen for all internal structural elements because of its material properties. Similar to the carbon composite material, titanium has a high specific strength

which helps with weight savings while maintaining the structural integrity of the aircraft. The titanium reinforcements will act as connection points since its ability to carry point loads is considerably better than the carbon composites. Another advantage to using titanium is the low galvanic potential between titanium and carbon composites; this minimizes the corrosion rate between the two materials resulting in lower maintenance costs.

A few reasons behind the use of high strength polycarbonate for the canopy is its impact resistance, durability, and scratch resistance. The impact resistance serves against debris impact such as bird strike or sand. The durability of the material reduces maintenance costs because it will not need to be replaced as often as a less durable material. The scratch resistance is important because of the sandy environment that the Cratus will be flying. If the canopy is scratched by the sand the visibility of the pilot will decrease.

The fuselage structure is shown below in Figure 11.1.

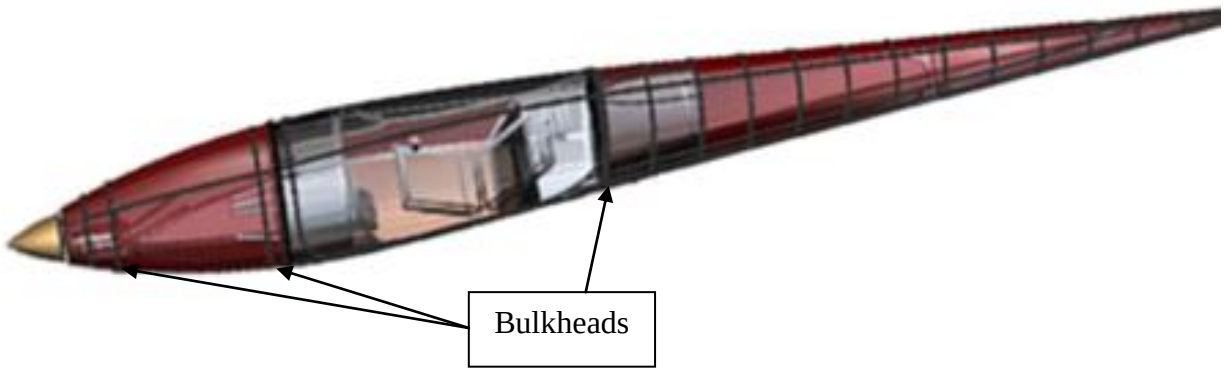

Figure 11.1: Fuselage Structure

11.2 Wing Structure

The structure of the wing, similar to the fuselage, will use carbon composites and titanium. Each wing will have titanium spars and ribs. The spars will be located at 0.2c and 0.7c and the ribs will be spaced every 18 inches span wise down the wing.

The aileron will be made of carbon fiber composite as a monocoque structure, assembled as a clam-shell. The forward wing spar will connect the wing to the aileron at 20% mgc. The counterbalance will be made of tungsten to improve the moment about the hinge.

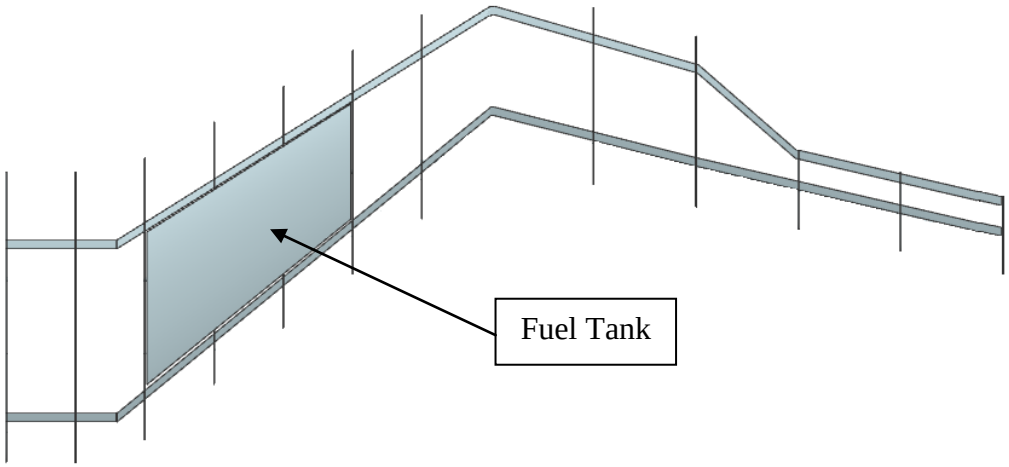

Figure 11.2: Wing Structure

An advantage of using carbon composites for the skin of the wing is its ability to adapt. The layup pattern for the outboard section of the wing will vary slightly from the inboard section to promote bend-twist coupling in the outboard section. This effect will only be employed in the outboard section because it is most critical for the outboard section to resist stall in high alpha flight to maintain controllability while the inboard section must retain its structural integrity.

11.3 Empennage Structure

The empennage structure will have a clam-shell monocoque skin made of carbon fiber composite. Each of the v-tail structures will have two spars located at 0.25c and 0.65c. These two spars will connect to the aft ring frames of the fuselage.

The ruddervator control surfaces will be constructed the same as the ailerons. They will be clam-shell monocoque skins with tungsten counterbalances. The forward spar of each structure will serve as connection points for the control surfaces. Figure 11.3 shows the structure of the empennage.

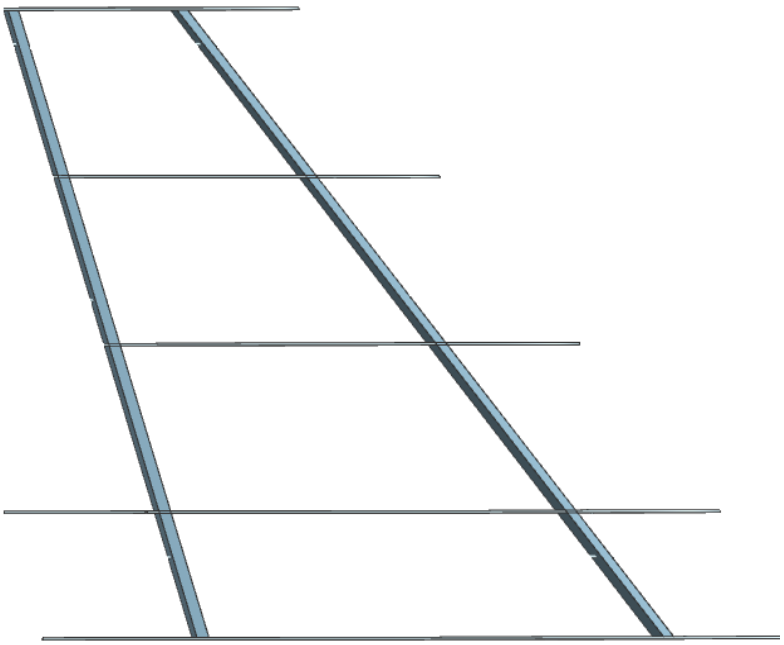

Figure 11.3: Empennage Structure

11.4 Engine Integration

The four hard points on the engine will be connected to the aft bulkhead. This connection will be made with shock absorbers to reduce vibrations from the engine. The engine connection to the bulkhead is shown below.

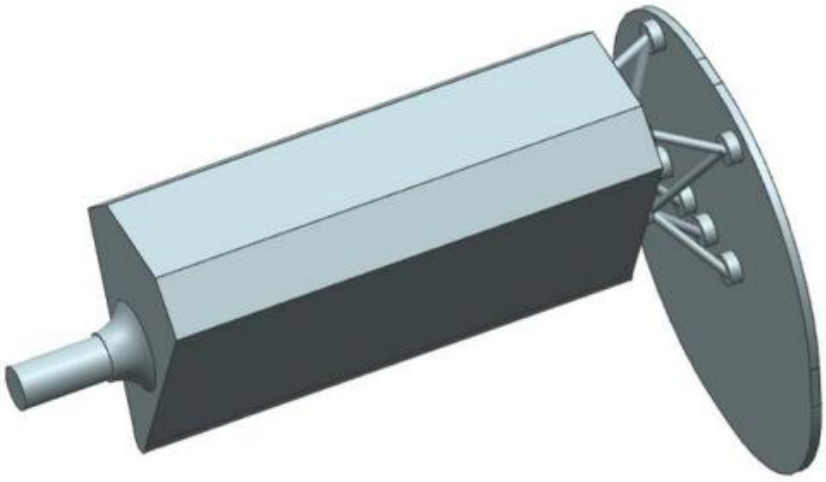

Figure 11.4: Engine Connection Points

Two keel beams will be added for structural support which will connect the forward bulkhead to the forward and aft wing spars below the engine for the wing engines. Two support beams will be added between the keel beams and bulkhead to resist deformation. The forward engine will also have two keel beams and support beams to connect the forward and aft bulkheads.

11.5 Final Structure

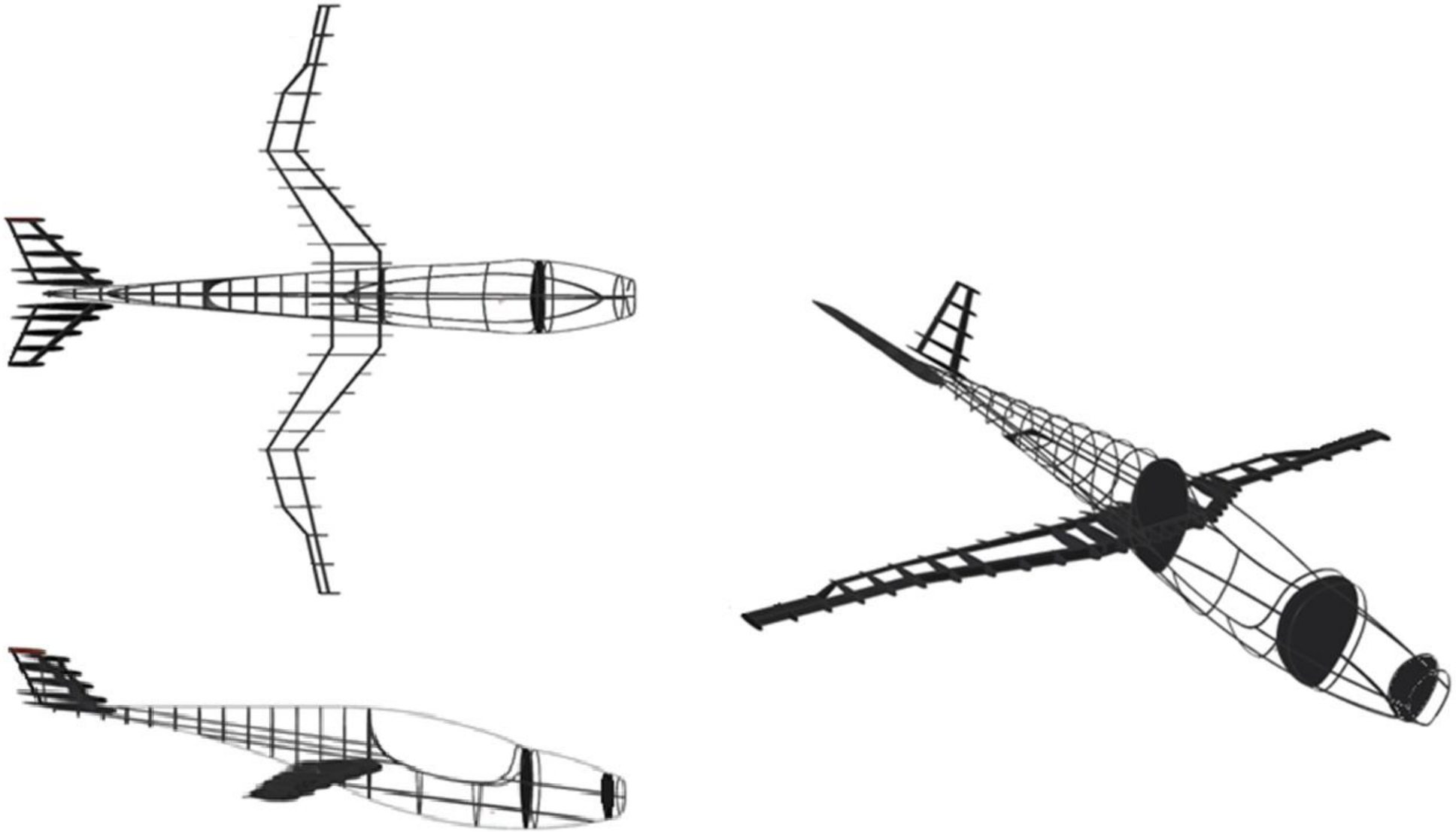

Figure 11.5: Final Structure (Scale 1:100)

12 Systems

The systems required by the Cratus include: flight control, fuel, electrical, and hydraulic. Each of these are explained further in the following sections.

12.1 Flight Control System

An irreversible flight control system was chosen for the Cratus for reliability, pilot control, and weight savings. To minimize risk of failure, each system has triple redundancy with one being wireless in the event that lines are severed. Each control system is split into three separate surfaces, controlled by each of the system redundancies. This is a safety feature in the event of a control system failure. If one system fails, the other two redundancies will maintain control of the aircraft.

The locations of the three redundant systems will be separated within the aircraft to decrease the chance of a total system failure. The single, wireless system will be within the center of each structure, while the other two system redundancies will run along the leading and trailing edge. This will prevent an intersection with the fuel tanks located within each wing.

Each of the actuators within the control surfaces will be located at the aerodynamic surface controls. This is done to maximize the stiffness of the structure at the connection point.

12.2 Fuel System

The required fuel volume of the Cratus will be split between three fuel storage tanks, two of which are located on the inboard section of the wings and one located within the fuselage. To allow for easier and faster refueling, a single fueling point is located on the inboard section of the left wing. A fuel line will run through the aircraft to join the three fuel tanks allowing

fuel transfer during fueling. A fuel vent is attached to each fuel tank with the two wing tanks being vented out the wingtips and the fuselage tank vented out the top of the fuselage. The fuel ventilation system will prevent the buildup of excess pressure within each of the fuel tanks.

Also attached to each of the wing fuel tanks is a sump. Since the wing tanks are at the lowest waterline station in the fuel system, unwanted contaminants will be drained from the system at these sump points.

As a safety precaution, the fuel lines will have self-sealing valves at the fuselage-wing connection. In the event that the wings shear from the fuselage of the aircraft, each of the fuel lines will self-seal preventing excess leakage of fuel. In addition, a valve will be located within each fuel line. The valve will be open during fueling and closed during flight. This will prevent fuel transfer during flight which is important to prevent weight change due to fuel movement during maneuvers.

12.3 Hydraulic System

For the brake system of the Cratus, a hydraulic system was used. Located next to the pilot, is a small piston which uses hydraulic fluid pressure to apply the force needed for the caliper braking system. The hydraulic system will also control the flight control system because hydraulic actuators were used.

12.4 Electrical System

The power requirements for the necessary electrical systems are listed in Table 12.1. A 2.1 A battery is required to support the listed systems with the listed loads. This is within a standard 12 V aircraft battery's limitations. The lines will be bundled with the flight control systems.

Table 12.1: Power Loads

System	Load
Avionics	12 W
Wing Navigation Lights	4.5 W
Tail Navigation Lights	3 W
Cabin Lights	1.5 W
Total	**25.5 W**

12.5 Exploded View

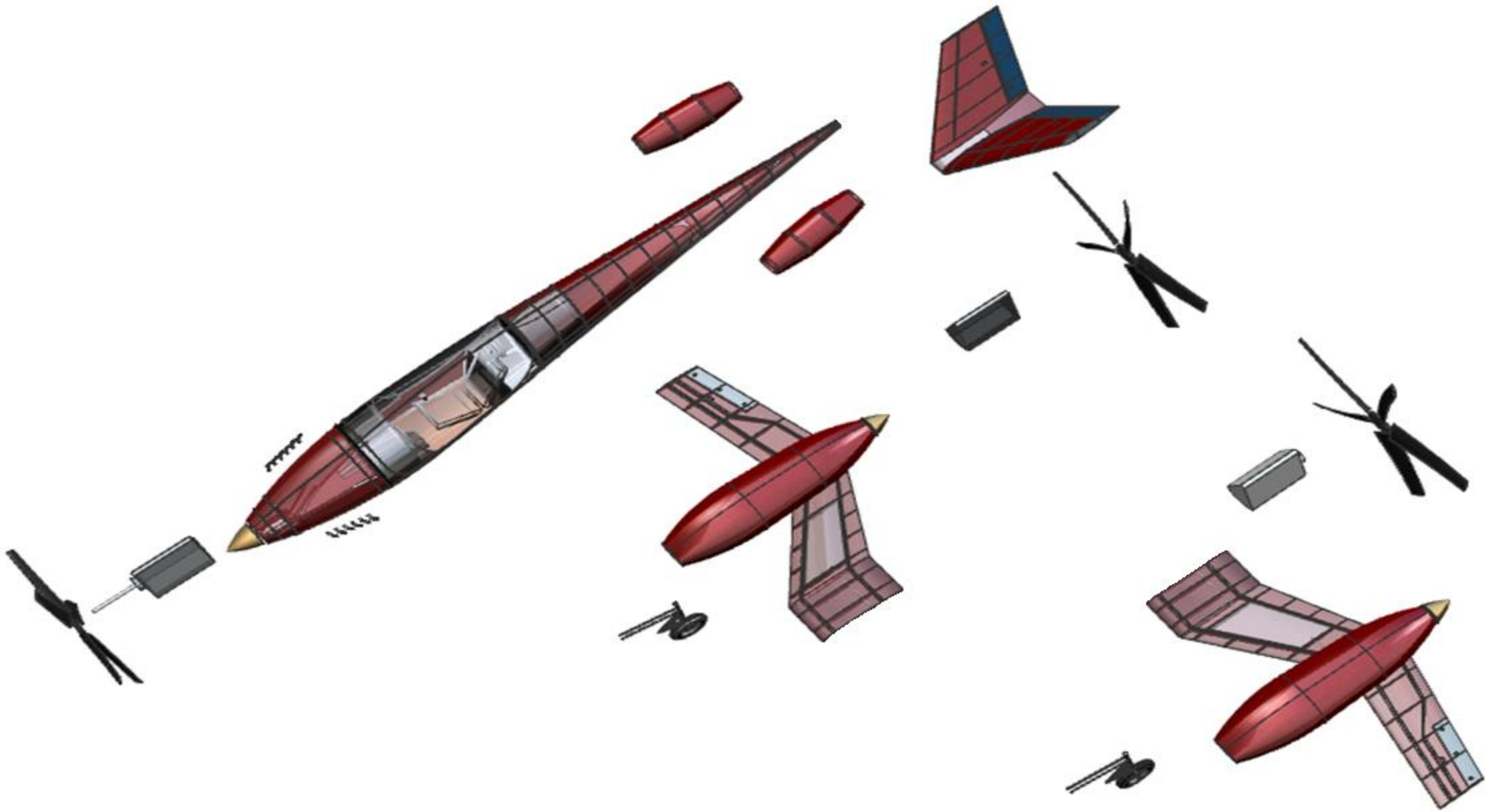

Figure 12.1: Exploded View

13 Advanced Technologies

In order to outperform the current Reno racers, the Cratus had to take advantage of advanced technology currently used in modern aircraft; these include: carbon fiber composite structure with titanium reinforcements, engine cooling methods, and engine-out safety procedures. Current racers are unable to take advantage of this technology, especially carbon fiber composite structure, because this change would require a complete overhaul of their aircraft, the equivalence of a new aircraft entirely. The Cratus was designed to join each of these technological advances into one aircraft, making it faster and more maneuverable than any other racer. The following sections explain further how the technology was used in the design of the Cratus.

13.1 Carbon Fiber Composite Structure

Carbon fiber composites were chosen for the skin of the entire aircraft based on their high specific strength, manufacturing properties, and aerodynamic properties. These were discussed more in depth in Chapter 10. Carbon composites are a relatively new material in the aerospace field in comparison to aluminums and other metals. They are becoming more common in all aspects of the field, from military to commercial, because of their material properties. Carbon composites are continually researched for possible improvements leading to various modifications, including the insertion of honeycomb between layers to increase compressive load resilience and various material substitutions including glass, aluminums, and other metals.

The Cratus inboard and outboard wing sections will both use carbon fiber composites, but with different layup patterns. By varying the ply orientation throughout the depth of the composite, various structural properties are attainable, such as: increased strength in the longitudinal, lateral, or diagonal load path. The structure can also become adaptable by placing

the plies in a manner which allows the structure to twist when a specific force is applied. This adaptive characteristic will be used in the outboard wing section of the Cratus. At high angles of attack, the force acting against the wing leading edge increases which would inherently cause a further increase in the angle of attack from the structure twisting under the load. This effect is typically exacerbated at the wingtip due to a lack of structure and the fact that it is at the wingtip. The Cratus will counteract this inherent destabilizing effect by using a composite ply layup which will cause the structure to inherently twist when high forces due to high angle of attack are encountered causing a decrease in the angle of attack at the wingtip, therefore preventing premature tip stall.

The high specific strength of carbon fiber composites allows structures to be built which would not be plausible with metals. The high aspect ratio wing of the Cratus would require significant internal structure to resist the forces acting on the structure with a conventional metal construction. This would increase the weight of the aircraft significantly. Carbon composites keep the strength of the structure while also cutting much of the structural weight which would otherwise be necessary.

13.2 Engine Cooling

As was explained previously, the Cratus will join together lost mass cooling and Meredith effect. Both of these have been used separately, but not together. Joining them increases the thrust output of the aircraft which helps to null the drag of the radiator and cooling. Although the rules state that the aircraft must be powered by a piston engine, many current racers use one of these effects or the other; therefore it is deemed to abide by the rules. Simply combining the two effects increases the efficiency of the aircraft.

13.3 Engine-Out Safety Procedure

Many current racers are powered by a single engine. There are many possible reasons for this, including: structural integrity of the aircraft, weight, or safety. Since the Cratus is built using titanium and carbon composites, there is more weight to use in areas other than structures, such as added power from an additional engine. An aircraft with laterally displaced engines introduces the possibility of a crash due to the yawing moment from one engine out operation. To reduce this risk, the electrical feathering system was implemented. This added system is possibly the most vital safety precaution on the Cratus. During a race, if an aircraft with laterally displaced engines has an engine failure the possibility of a safe emergency landing is extremely unlikely. Many pilots shy away from aircraft which introduce engine out safety hazards (Ref. 3). By using an electrical feathering system to reduce yawing moment from an engine failure, pilots would be more willing to fly the Cratus (Ref. 3).

14 Cost Estimation

The rules for the Reno Races state that there is no cost requirement for entries, this was reiterated in the RFP (Ref. 2). For design completeness, a costing analysis was done for the Cratus and a business strategy was created.

Assuming the Cratus is only used as a Reno racing aircraft, theoretically only one aircraft would need to be produced, not considering testing. This would result in extremely high production costs, as is explained later; therefore full production run costs were estimated.

The costing analysis per airplane was completed using AAA for 1, 10, 100, and 1,000 aircraft production runs, these values are shown in Table 14.1.

Table 14.1: Costing Analysis

Number of Aircraft Produced	Price per Aircraft ($, millions)
1	204
10	37.8
100	11.9
1000	5.78

The values above show the sharp decrease in price per aircraft following a production output of one aircraft. This relationship is shown graphically in Figure 14.1.

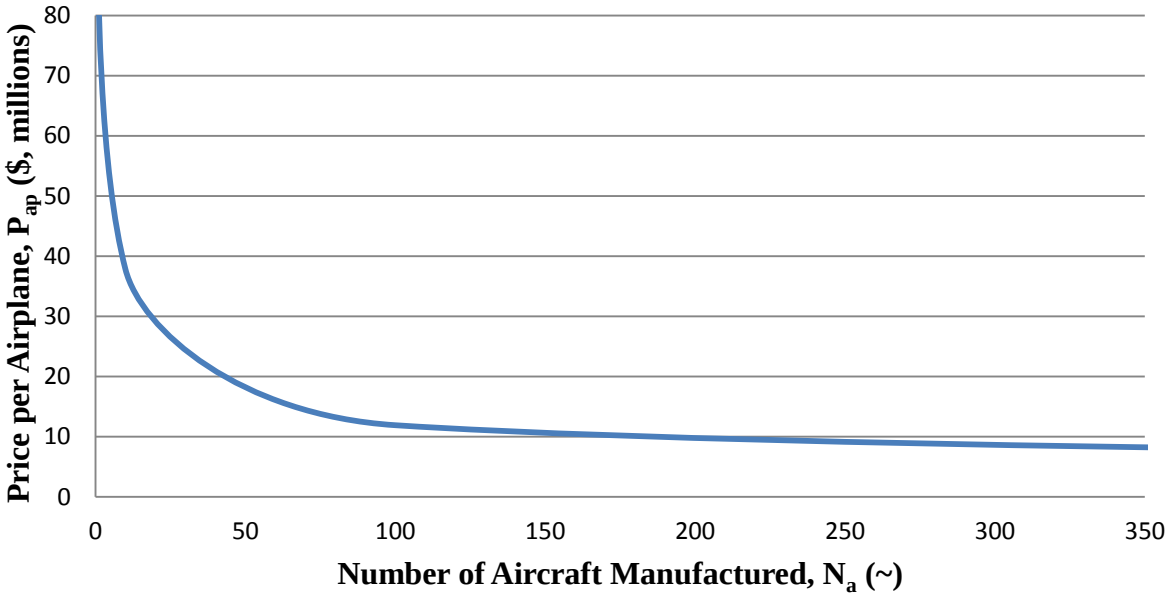

Figure 14.1: Costing Relationship

As can be seen in Figure 14.1, there is a significant price decrease in all production runs which are greater than one aircraft being produced. It should be noted that these values account for a 10% profit in all production runs after 10 aircraft. This is representative of the Cratus entering the market as a military trainer aircraft rather than just a racer.

Another notable aspect of the costing relationship shown in Figure 14.1, is the risk involved in production of the Cratus. In the event of lacking sales, the price per airplane is significantly higher. This increased price could lead to further decrease in sales. To combat this risk, an analysis of similar aircraft currently in service was performed. These aircraft are shown below.

Aircraft	Number Produced	Unit Cost	Maximum Speed	Range	Operators
EMB 314	Over 700	$9 million	346 mph	974 miles	Brazil Burkina Faso Chile Colombia Dominican Republic Ecuador El Salvador Guatemala Indoneis Lebanon
KT-1	Over 100	$4.7 million	357 mph	828 miles	Indonesia Republic of Korea Turkey
T-6	Over 435	$6 million	346 mph	1,036 miles	Canada Germany Greece Israel Iraq Morocco United States
PC-21	Over 26	$9 million	428 mph	828 miles	Singapore Switzerland United Arab Emeriates

Upon comparison of the above aircraft, it can be seen that there is an average unit cost of approximately $7 million, with a maximum speed of 375 mph and a range of 920 miles. Based on these values the Cratus would be able to fly considerably faster than any of these aircraft. The range of the Cratus is small for the Reno Races, but the fuselage area allows room for an additional optional fuel tank. This would increase the range of the Cratus to 1,150 miles. This range would beat all of the compared aircraft. When comparing the price per unit for the aircraft, the number produced must be considered. As was seen in Figure 14.1, the price per unit and number produced were extremely dependent on each other. The total sum of the similar aircraft produced is over 1,260 aircraft. It was assumed that a similar number of Cratus would be manufactured since the goal is to take over the piston-engine, propeller-driven military trainer market. The price per unit would be $5.78 million if roughly the same number of Cratus are manufactured. This cost is less than three of the four similar aircraft. Assuming the price difference between the Cratus and KT-1 results in the loss of roughly 100 aircraft in the manufacturing rate, the price per unit is still less than the other three similar aircraft.

The Cratus' marketing strategy will be speed, range, and cost. As was explained above, the Cratus will be able fly faster and further than similar aircraft for smaller cost. This makes it a lucrative sell for governments looking to acquire a low cost high yield aircraft to outperform its competitors. The Cratus will provide jet-like performance in speed and range for the maintenance cost of a piston aircraft.

The advantage in the Cratus entering the market as a Reno Racer is publicity. The Reno Races will not only serve as a competition for the Cratus, they will also be advertisement for the performance of the aircraft. Since the high speeds it was designed for can beat all current Reno racers, the Cratus will be able to prove its performance with competition wins. This is

important in selling aircraft because it provides undisputable evidence of the aircraft's performance. This will theoretically increase sales, which will lead to a reduction in the unit price.

15 Final Disposition

The Cratus Racer was designed to optimize technology now available for aircraft design. By taking advantage of advanced materials, engine cooling techniques, and improved emergency protocol, the Cratus can fly faster than any current racer while also taking every precaution for pilot and spectator safety.

The Cratus also goes above and beyond Reno Racing. It is a viable option in the military trainer market. It can fly faster and further, with the reserve fuel tank, than currently used trainers for a fraction of the cost.

16 References

1. Anon., "National Championship Air Races and Air Show," *National Championship Air Races*, http://airrace.org.
2. Anon., "2011-2012 AIAA Foundation Undergraduate Individual Aircraft Design Competition", *American Institute of Aeronautics and Astronautics*, http://www.aiaa.org.
3. Brungart, J., "Discussion about Pilot Preferences", Technical Discussion, March 2012.
4. Roskam, Jan, *Airplane Design Series*, DARcorporation, Lawrence, KS, 2005.
5. Anon., "Exciting Racing Action," *National Championship Air Races*, http://www.airrace.org/at_the_races/racing.php.
6. Anon., "The Vickers Viscount", *The Wings of the Web*, http://www.airliners.net/aircraft-data/stats.main.
7. Andrews, Mark, "How does background noise affect our concentration?", *Scientific American Magazine*, January 2010.
8. Johnston, M., "Unlimited Class", *Airplanes*, http://www.galleries.intsysint.com/Airplane.
9. Roskam, Jan, *Airplane Design: Part I, Preliminary Sizing of Airplanes*, DARcorporation, Lawrence, KS, 2005.
10. Roskam, Jan, *Airplane Design: Part V, Component Weight Estimation*, DARcorporation, Lawrence, KS, 2005.
11. Roskam, Jan, *Airplane Design: Part IV, Layout of Landing Gear and Systems*, DARcorporation, Lawrence, KS, 2005.
12. Roskam, Jan, *Airplane Design: Part VI, Preliminary Calculation of Aerodynamic, Thrust and Power Characteristics*, DARcorporation, Lawrence, KS, 2005.

13. BMW Sauber F1 Team, “BMW F1 Engine Comparison: V8 vs. V10”, *MWerks Forums*, March 2006, http://www.mwerks.com/artman/publish/features/printer_982.shtml.
14. Grosveld, F.M.W.A., "The Application of the Prop-Fan Concept in Preliminary Design of a Very Advanced Light Technology Twin (VATLIT)," American Institute of Aeronautics and Astronautics, AIAA-79-1343, AIAA/SAE/ASME 15th Joint Propulsion Conference, Las Vegas, Nevada, June 18 - 20, 1979.
15. Lan, C.T.E., and Roskam, J., "Airplane Aerodynamics and Performance," Propeller Theory, DARcorporation, Lawrence, Kansas, 1980.
16. Farokhi, S., “Aircraft Propulsion,” The University of Kansas, Lawrence, KS, 2009.
17. Farokhi, S., "Thrust Addition from Ram-Rocket Configurations," The University of Kansas, Lawrence, KS 29 April 2012.
18. Roskam, Jan, *Airplane Design: Part VII, Determination of Stability Control and Performance Characteristics: FAR and Military Requirements*, DARcorporation, Lawrence, KS, 2005.